EJN European Journal of Neuroscience FENS Federation of European Neuroscience Societies

EARLY SENSITIVITY OF EVOKED POTENTIALS TO SURFACE AND VOLUMETRIC STRUCTURE DURING THE VISUAL PERCEPTION OF THREE-DIMENSIONAL OBJECT SHAPE

Journal:	*European Journal of Neuroscience*
Manuscript ID	EJN-2017-11-25086(EVPO).R2
Manuscript Type:	Special Issue Article
Date Submitted by the Author:	n/a
Complete List of Authors:	Leek, Charles; University of Liverpool, Faculty of Health and Life Sciences, School of Psychology Roberts, Mark; Bangor University, Psychology Dundon, Neil; University of California Santa Barbara, Psychological and Brain Sciences Pegna, Alan; University of Queensland Faculty of Health and Behavioural Sciences, School of Psychology
Key Words:	Evoked potentials, N1, PERCEPTUAL GROUPING, 3D SHAPE, perception

To: Profs John Foxe & Paul Bolam
co-Editors in chief, EJN

September 11th, 2018

Manuscript Number: EJN-2017-11-25086(EVPO).R1

EARLY SENSITIVITY OF EVOKED POTENTIALS TO SURFACE AND VOLUMETRIC STRUCTURE DURING THE VISUAL PERCEPTION OF THREE-DIMENSIONAL OBJECT SHAPE

Thank you for your decision letter of August 16th, 2018.

We are grateful for your (and the reviewers) positive response to our revised paper. You had requested one further minor revision concerning the rationale for using a multi-method approach to the analyses. In short, we adopted this approach to verify the robustness of any observed effects across different approaches to the analysis of EEG signals. We have addressed this point in version R2, and specifically clarifying the unique contribution of the topographic segmentation approach. The revisions are highlighted in yellow in the text on page 10 under a new sub-heading 'ERP data analysis: Multi-method approach.

We very much hope that these revisions are satisfactory.

Sincerely,

Charles Leek PhD CPsychol AFBPsS FHEA

Head of Institute of Life and Human Sciences

Professor of Cognitive Neuroscience, School of Psychology

University of Liverpool

R220 Eleanor Rathbone Building, Bedford Street South, Liverpool, L69 7ZA

Tel: 0151 795 7650 | Email: charles.leek@liverpool.ac.uk

EARLY SENSITIVITY OF EVOKED POTENTIALS TO SURFACE AND VOLUMETRIC STRUCTURE DURING THE VISUAL PERCEPTION OF THREE-DIMENSIONAL OBJECT SHAPE

E. Charles Leek[1] Mark V. Roberts[2] Neil M. Dundon[3] & Alan J. Pegna[4]

[1] School of Psychology, Institute of Life and Human Sciences, University of Liverpool, UK

[2] School of Psychology, Bangor University, Bangor, UK

[3] Brain Imaging Center, Department of Psychological and Brain Sciences, University of California, Santa Barbara, USA

[4] School of Psychology, University of Queensland, Queensland, Australia

RUNNING HEAD: EVOKED POTENTIALS AND SHAPE PERCEPTION

KEYWORDS: EVOKED POTENTIALS, N1, PERCEPTUAL GROUPING, 3D SHAPE PERCEPTION

WORD COUNT: 7871

Address for Correspondence:

Charles Leek PhD, School of Psychology, Institute of Life and Human Sciences, University of Liverpool, Liverpool, L69 7ZA, UK: Email: Charles.Leek@liverpool.ac.uk

ABSTRACT

This study used event-related potentials (ERPs) to elucidate how the human visual system processes three-dimensional (3D) object shape structure. In particular, we examined whether the perceptual mechanisms that support the analysis of 3D shape are differentially sensitive to higher-order surface and volumetric part structure. Observers performed a whole-part novel object matching task in which part stimuli comprised sub-regions of closed edge contour, surfaces or volumetric parts. Behavioural response latency data showed an advantage in matching surfaces and volumetric parts to whole objects over contours, but no difference between surfaces and volumes. ERPs were analysed using a convergence of approaches based on stimulus dependent amplitude modulations of evoked potentials, topographic segmentation and spatial frequency oscillations. The results showed early differential perceptual processing of contours, surfaces and volumetric part stimuli. This was first reliably observed over occipitoparietal electrodes during the N1 (140-200ms) with a mean peak latency of 170ms, and continued on subsequent P2 (220-260ms) and N2 (260-320ms) components. This differential sensitivity in perceptual processing during the N1 was accompanied by distinct microstate patterns that distinguished among contours, surfaces and volumes, and predominant theta band activity around 4-7Hz over right occipitoparietal and orbitofrontal sites. These results provide the first evidence of early differential perceptual processing of higher-order surface and volumetric shape structure within the first 200ms of stimulus processing. The findings challenge theoretical models of object recognition that do not attribute functional significance to surface and volumetric object structure during visual perception.

Word count: 240

INTRODUCTION

Object shape perception in human vision is remarkably robust to variability in sensory input caused by changes in luminance, shadow, viewpoint and scale (e.g., Arguin & Leek, 2003; Biederman, 1987; Harris, Dux, Benito & Leek, 2008; Hummel, 2013; Hummel & Biederman, 1992; Leek, 1998a; 1998b; Marr & Nishihara, 1978; Pizlo, 2008; Riesenhuber & Poggio, 1999; Serre, Oliva & Poggio, 2007; Tarr & Bulthoff, 1995). One fundamental, and unresolved, issue is what kinds of shape information mediate this robust perceptual processing of complex object shape (e.g., Hummel, 2013; Kubilius, Wagemans & Op de Beeck, 2014; Tarr & Bulthoff, 1995).

During its early stages, object shape processing is largely assumed to be based on local edge features coded via the response patterns of orientation sensitive neurons in primary visual cortex (e.g., Carandini et al., 2005; Hubel & Wiesel., 1962). Consistent with this several approaches to shape perception attribute a key role for edge (or contour)-based feature descriptors in low-level shape representation (e.g., Pizlo, 2008; Riesenhuber & Poggio, 1999; Serre, Oliva & Poggio, 2007). What is less clear is whether the perceptual system also makes use of higher order geometric primitives during the processing of complex three-dimensional (3D) object shape (e.g., Hummels, 2013; Leek, Reppa & Arguin, 2005; Reppa, Greville & Leek, 2015). On the one hand, it has recently been shown that low-level edge-based descriptors may be sufficient to recover veridical representations of 3D object structure when combined with geometric simplicity constraints (e.g., Pizlo, 2008). In addition, elsewhere, remarkable performance in image classification has been demonstrated in hierarchical, feedforward, multilayer networks which compute shape based on increasingly complex edge-based features, or multi-dimensional image descriptors (e.g., SIFT), without explicit representation of higher order geometric structure (e.g., Kheradpisheh, Ghodrati, Ganjtabesh et al., 2016; Krizhevsky, Sutskever & Hinton, 2012; ;

LeCun, Bengio, & Hinton, 2015; Riesenhuber & Poggio, 1999; Serre, Oliva & Poggio, 2007). Other work has provided evidence for the sensitivity of higher visual areas to increasing feature complexity – for example, angle or curvature in V2 (Dobbins et al., 1987; Ito & Komatsu, 2004) and to more complex curved contour fragments in V4 (e.g., Pasupathy & Connor, 1999; Yamane et al., 2008). On the other hand, several prominent theories of object recognition posit that beyond edge-based image descriptors, the visual system also computes surfaces and/or volumetric primitives (e.g., Biederman, 1987; Hummel, 2013; Hummel & Biederman, 1992; Leek, Reppa & Arguin 2005; Marr & Nishihara, 1978; Reppa, Rodriguez & Arguin, 2009). For example, using a part-deletion paradigm, Biederman (1987) has shown that object naming performance varies as a function of the number of visible volumetric components – evidence that has been taken to support the hypothesis that 3D object perception involves the derivation of volumetric parts and their spatial configuration within a structural description. In other work, the organisation and structure of this higher-order representational structure has been studied using behavioural measures of whole-part matching and repetition priming (e.g., Leek, Reppa, & Arguin, 2005; Leek, Reppa, Rodriguez, & Arguin, 2009). For example, Leek et al. (2005) showed that response latencies to match stimuli comprising sub-sets of 3D object contours decreased for part stimuli corresponding to spatially adjacent object surfaces compared to perceptually closed but ungrouped contour stimuli. Interestingly, also, observers were equally efficient in matching surface-based parts, and volumetric components, to whole objects. That is, there was no perceptual advantage found for whole-part matching of volumes over surface primitives. From these findings, Leek et al (2005) outlined a hierarchical model of image classification that contained a level of representation of object surfaces defined by polygons of edge-bounded closed contour. In that model, higher-order surface, but not volumetric, shape primitives play a fundamental role in 3D object representation. Some other models

contain levels of representation for both surface and volumetric shape primitives within a hybrid framework (e.g., Hummel, 2013; Hummel & Stankiewicz, 1996).

Surprisingly, there is very little evidence about the potential differential processing of these higher-order shape primitives, and current studies have relied on overt measures of behavioural performance (e.g., naming or whole-part matching response latencies). Additionally, there have been no prior studies about the time course of any differential perceptual sensitivity to these higher-order shape primitives in the context of 3D object processing. The high temporal resolution of event-related potentials (ERPs) provides an opportunity to measure implicit differential perceptual processing of 3D object structure, elucidate the time course of processing, and to test theoretical hypotheses about the organisation and structure of 3D object representations. In recent work using ERPs, it has been shown that, relatively early during the perceptual processing of 3D object shape, signal amplitudes are differentially modulated by global and local shape similarity (Leek, Roberts, Oliver, Cristino & Pegna, 2016; Oliver, Cristino, Roberts, Pegna & Leek, 2017; Pegna, Darque, Roberts & Leek, 2017). For example, Oliver et al (2017 – see also Leek et al., 2016) found distinct patterns of ERP modulation over posterior electrodes on an N1 component (145-190ms post-stimulus onset) reflecting differential processing of global and local (part-based) 3D object similarity. This suggests that global and local shape structure is computed relatively early during the perceptual analysis of 3D object shape. What remains less clear is whether this analysis distinguishes among different kinds of higher-order geometric shape primitives.

The aim of the current study was to examine this issue using ERPs to provide a high temporal resolution and implicit measure of perceptual processing. We used the same whole-part matching task, and stimulus sets, reported in the study by Leek et al (2005). Observers made whole-part matching judgements about novel objects defined by edge

contour, and without surface rendering. Part comparison stimuli comprised either bounded (i.e., perceptually closed) regions of contour, surfaces or volumes. Our goal was to examine whether the early N1 component associated with differential processing of global and local object shape shows differential sensitivity to higher-order surface and volumetric structure. Theoretical models – like some variants of recent feedforward deep network approaches, which do not attribute functional significance to these kinds of shape primitives would not predict the perceptual system to show differential sensitivity. In contrast, models that contain levels of higher-order shape representation in which surface and/or volumetric structure is made explicit predict differential sensitivity during object shape perception.

METHOD

Participants

Twenty-three participants (Mean age 24.65; SD = 5.4; N = 14 female; 22 = right handed) from Bangor University completed the study for course credit. The sample size estimate was derived from the previous work of Leek et al (2005, Exp. 3; N=20) using the same paradigm. The additional three participants were included to provide some flexibility in the event of bad EEG recordings. In the event, all tested participants were included in the analyses. All participants reported having normal or corrected to normal visual acuity, and no history of neurological or psychiatric disorder. The study protocol was approved by the Bangor University (School of Psychology) Research Ethics Committee and in full accordance with the ethical guidelines of the British Psychological Society and World Medical Association Declaration of Helsinki. Informed consent was obtained from all participants.

Apparatus

EEG signals were acquired using a 64-channel NeuroScan SynAmps2 system (Neuroscan Inc.) - see below for acquisition and online/offline filtering parameters. The EEG data were recorded in a fully shielded and sound attenuated room. Two Dell Precision 380 workstations controlled stimulus presentation and data acquisition. Stimuli were displayed on a Hitachi 17" CRT monitor running at 1280 x 1024 (32 bit colour depth) resolution. A standard QWERTY PC keyboard was used to acquire behavioural responses. The experiment was programmed and run using E-prime (v.1.1; www.pstnet.com/eprime).

Stimuli

The stimuli comprised a set of 12 line drawings of 3D novel objects (See Figure 1). These were the same object sets and part feature stimuli used in Leek et al (2005, Exp. 3).

INSERT FIGURE 1 ABOUT HERE

Opaque line drawings were used to avoid ambiguity about edge boundaries (e.g., that might arise from surface rendering with shadow). Each object was scaled to fit within a 6x6 cm frame that subtended 4.29° visual angle (vertically and horizontally) from a viewing distance of 80cm. The whole objects consisted of two volumetric components – a larger principal component and a smaller component. For each object, two variants for each of three types of part feature stimuli were generated: Contour, Surface and Volume. The contour part stimuli (N=24) were made by deleting regions of edge contour in the whole object model under the constraint that the resulting stimulus consisted of a perceptually closed form containing edge contour from both volumetric components (see Figure 1). These stimuli provided a 'low-level' edge-based 'baseline' feature condition. The volumetric part stimuli (n=24) each consisted of a single volumetric component. The surface part stimuli (N=24) consisted of 2D surface patches (defined as polygonal bounded regions of edge contour) – see Figure 1. Construction of the surface part stimuli followed two constraints: (1) Surface parts were each exactly matched to the respective volumetric parts (from the same whole object stimulus) for the number of visible surfaces shown; (2) Surfaces were spatially contiguous; that is, they each shared a common boundary with another surface. This ensured that any differences between surface and volume feature type could not be accounted for in terms of either the number of visible surfaces shown or surface spatial contiguity. We also computed values for two other stimulus properties: (1) visible edge contour and (2) vertices (defined as intersections between any two contours). For edge contour we measured the total visible

contour in each part stimulus as a function of stimulus condition. This was done using the 'ImageJ' processing package (https://imagej.nih.gov/ij/). The mean visible edge contour was: Contour (M = 14.62cm; SD = 3.10); Surface (M = 16.75cm; SD = 2.47); Volume (M = 14.94cm; SD = 3.35). A One-way ANOVA across stimuli was significant; F (2, 22) = 11.47, $p < .001$. Post-hoc tests using the Fisher LSD showed that there were significant differences ($p < .05$) in mean edge contour between the Contour and Surface and Volume and Surface conditions. There was no difference in mean edge contour between the Contour and Volume conditions. The mean number of visible vertices per part stimulus was: Contour (M = 9.00; SD = 1.26); Surface (M = 6.67; SD = 0.72); Volume (M = 8.92; SD = 1.24). A Friedman One-way ANOVA on these values was significant $\chi 2$ (N = 12, $d.f.$ = 2) = 14.65, $p < .001$). Paired contrasts using the Wilcoxen test showed significant differences between Contours and Surfaces T = 2; Z = 2.9, p = .005; and between Surfaces and Volumes T = 10; Z = 2.27, p = .02. There was no significant difference in vertex count between the Contour and Volume conditions. Whole object displays were enlarged to 150% of their original size to prevent contour overlap with the part stimuli. This was done to prevent participants from completing the task using a direct pixel-to-pixel matching strategy.

Design and Procedure

Following Leek et al (2005; Exp. 3) the study used a 2 (Match vs. Mismatch) x 3 (Feature type: Contour, Surface, Volume) repeated measures design. There were 288 trials (144 match and 144 mismatch) comprising 48 trials per condition. In total, each whole object (N=12) was presented 24 times (12 times in Match and 12 times in Mismatch trials). Each part stimulus (N=24) was presented 12 times. For match trials each part stimulus was presented with its corresponding whole object. For mismatch trials whole-part stimuli were randomly assigned (within conditions). There were four blocks of 72 trials. Participants were also shown 12 practice trials (6 match and 6 mismatch) using stimuli that were not presented during the

experimental trials. Participants completed two blocks responding 'Match' with the right hand, and 'Mismatch' with the left, and two blocks with the reverse response-hand assignment. Response-hand assignment order was counterbalanced across participants (half started with right/left and the other half with left/right). The trial sequence and stimulus timing are shown in Figure 2. The task used a whole-part matching paradigm involving the initial presentation of a whole object stimulus (S1 stimulus - 1200ms) followed by a part comparison (S2 stimulus - 3s). There was a blank ISI of 750ms between the S1 and S2 stimuli. Observers were instructed to decide whether the part comparison (S2) stimulus matched or mismatched any part of the shape of the S1 (whole object) stimulus. They were instructed to respond as quickly and accurately as possible. The experiment lasted about 60 minutes.

INSERT FIGURE 2 ABOUT HERE

Electrophysiological Recording and Processing

EEG signals were sampled at 1024 Hz from 64 Ag/AgCl electrodes referenced to Cz and placed according to the extended 10–20 convention (American Electroencephalographic Society, 1991: TP7, FT7, AF7, FCz, AF8, FT8, TP8, C5, F5, AF3, CPz, AF4, F6, C6, CP3, C1, FC3, POz, FC4, C2, CP4, TP9, PO7, P5, Oz, P6, PO8, TP10, P1, PO3, PO4, P2, FT9, F7, Fp1, AFz, Fp2, F8, FT10, T7, FC5, F3, Fz, F4, FC6, T8, CP5, C3, FC1, Pz, FC2, C4, CP6, P7, P3, CP1, O1, CP2, P4, P8, Iz, PO9, O2, PO10). Impedances were below 9kΩ. Signals were filtered on-line between 0.01 and 100 Hz, data were filtered off line using a 30 Hz low pass filter (except for the time frequency analysis – see below) with a slope of 12 db/oct. Ocular artifacts were mathematically corrected using Scan 4.3 software (Neuroscan, Inc.) based on an algorithm developed by Gratton, Coles & Donchin (1983). Remaining artifacts

were manually rejected upon visual inspection. EEG epochs ranging from -100 to 900ms relative to stimulus onset were baseline corrected in reference to pre-stimulus activity before ERP averaging. Finally, ERPs were re-referenced to the global average reference. Peak detection was carried out automatically, time-locked to the latency of the peak at the electrode of maximal amplitude on the grand average ERP (Picton et al., 2000). Triggers were recorded during EEG data acquisition marking the whole object (S1) and part stimulus (S2) onset, feature condition and response accuracy.

ERP data analyses: General Principles

In light of the recent guidelines described by Luck and Gaspelin (2017) in relation to the issue of multiple comparisons/false discovery rate in electrophysiological studies, we adopted a *highly conservative* approach to the ERP data analyses. The analyses were constrained *a priori* in several ways. (1) Standard waveform analyses were restricted to ERP amplitude data, and do not include analyses of latency. This is motivated on the grounds that our theoretical hypotheses make no specific predictions about latency; only whether or not we expect to observe modulations of evoked potentials related to the factor of feature (part) type. (2) For the same reason, we do not attribute functional significance to the polarity of amplitude modulations between conditions. (3) We restricted our analyses of waveform amplitude to the four main early components P1, N1, P2 and N2 which can be clearly identified based on the topography, deflection and latency characteristics of the respective grand averages time-locked to part stimulus (S2) presentation. Additionally, this choice is further motivated by other recent ERP studies of visual object processing that have identified those four main components in the perceptual analysis and recognition of 3D object shape (Leek et al., 2016; Oliver et al., 2017; Pegna et al., 2017). (4) We restricted the decomposition of statistical interactions in the ERP amplitude data only to those involving the main factor of theoretical interest – feature type. (5) Statistical corrections to *p* values

were applied where appropriate, and significance tests were conducted on the time frequency data relative to a bootstrapped random distribution via permutation analyses. These a *priori* constraints were adopted to reduce the prospective Type 1 (false discovery) error rate. All analyses of ERP data were conducted on correct response trials only.

ERP data analyses: Multi-method approach

We also wanted to extend our investigation beyond standard analyses of ERP waveform amplitudes, and to examine whether any observed differential perceptual sensitivity to higher-order shape structure would also be manifest in topographic microstates and the frequency domain. We describe our approach to the standard waveform, topographic segmentation and time frequency analyses below:

Standard Waveform Analyses

The four main early visual ERP components P1, N1, P2 and N2, were identified based on the topography, deflection and latency characteristics of the respective grand average ERPs time-locked to S2 (part) stimulus onset. Epochs of interest for each component were defined on the basis of deflection extrema in the mean global field power (MGFP) (Picton et al., 2000). Peak detection was time-locked to the electrode of maximal amplitude for each component; P1: 70 to 130ms maximal at electrode PO8 (mean peak 100ms); N1: 140 to 200ms maximal at electrode P6 (mean peak 170ms); P2: 220 to 260ms maximal at electrode Pz (mean peak 240ms); and N2: 260 to 320ms maximal at electrode P4 (mean peak 280ms). Peak mean amplitudes and latencies were analysed using 3 (Feature: Contour, Surface, Volume) x 2 (Match, Mismatch) x LATERALITY (Right, Left) for P1/N1 and (Centre, Right, Left) for P2/N2/P3 as factors in repeated measures ANOVA. Electrodes used for each component were: P1: PO7, P5, P7, P6, P8, PO8; N1: PO7, P5, P7, P6, P8, PO8; P2: P1, PO3, PZ, POZ, P2, PO4; and N2: P1, PO3, P3, CPZ, PZ, POZ, P2, PO4, P4. Channel selection was based on

initial inspection of the topographies with electrode clusters centred on the site showing the peak amplitudes within the selected time window for each component with a corresponding cluster in the opposite hemisphere. Greenhouse-Geisser corrections were applied to ERP data analyses to compensate for violations of sphericity. Unless otherwise stated only significant main effects and interactions are reported where corrected $\alpha < .05$. Exact values of p are reported, except where $p < .001$ (two tailed).

Temporal segmentation

In addition to waveform analyses, we performed a spatiotemporal segmentation on the grand average of the Contour, Surface and Volume conditions of the Match situation, in order to determine whether the N170 scalp topographies differed across conditions.

At each successive time point of an ERP, the amplitude values of every electrode can be colour coded on a schematic representation of the scalp. In this manner, a map can be drawn representing the spatial distribution of the scalp potential at a specific period in time. Interestingly, when observing the succession of maps in an ERP, it has been noted that map series does not fluctuate randomly but is composed of topographies that remain stable for periods of time of the order of tens to hundreds of milliseconds (Lehmann, 1987; Lehmann et al., 2009; Michel et al., 2001). Different topographies measured at the surface of the scalp obviously reflect the activation of different neuronal assemblies (Vaughan, 1982), suggesting that periods of stable maps may be due to the ongoing activity of a particular neuronal distribution. These stable topographies, called microstates (Lehmann et al., 2009), are thus posited to correspond to periods during which given neural networks are engaged in a specific step of information processing (Brandeis & Lehmann, 1986; Lehmann & Skrandies, 1984; Michel et al., 1999; Michel et al., 2001).

The idea behind topographic segmentation is to identify the succession of microstates underlying the ERP map series. In the current study, the comparison of the microstates composing in our different conditions should thus inform us whether the networks processing the stimuli are similar or not. This approach allows us to identify whether any changes emerging from the waveform analysis are due strictly to differences in the amplitudes of the components (that are otherwise similar in their overall spatial pattern), or whether these differences are accompanied by simultaneous, differential changes in activity over other electrodes as well, i.e., correspond to changes in scalp topography. Differences in scalp topography would indicate the activation of distinct networks for the processing for the Contour, Surface or Volume conditions, while this would not necessarily be the case for similar topographies. The microstates present in the ERP map series of the grand averages were determined using a topographic atomize and agglomerate hierarchical clustering algorithm (Murray et al., 2008). In order to establish the optimal number of maps, explaining the map series, a measure based on the Krzanovski–Lai (KL) criterion was used (Tibshirami and Walther, 2005). This criterion examines the quality of the segmentation using a measure of dispersion (W), which produces a value that approaches 0 as the quality of the segmentation increases, i.e., as the number of segments increases, so does the quality of the segmentation. However, as this number continues to increase, the deceleration in the W curve flattens out, forming as “elbow”, at which point the deceleration decreases. This point is taken as an indication that any additional maps no longer meaningfully increase the quality of the segmentation procedure. In the adaptation of the procedure used here (Murray et al., 2008), the KL measure was adapted to be a relative measure of curvature such that its highest value should in principle indicate the optimal number of clusters explaining the map series. Maps lasting less than 20ms were rejected and topographies were merged if their correlation exceeded 90%.

The second step of analysis consisted in determining the statistical validity of the maps extracted from the grand averages. To this effect, the amount of variance that the microstate maps explained in the ERPs of very individual was computed within the N1 time window of each condition (explained variance was computed as the sum of products of values for the segment map and the individual's map at every electrode squared, divided by the product of the sum of squared values at each electrode of both maps). The values of the explained variance were then explored statistically using non-parametric statistics (Friedman's Analysis of Variance or Wilcoxon's matched pairs test) to compare experimental condition (Murray et al., 2008). Segmentation analyses were performed using Cartool software (Brunet et al., 2011).

Time Frequency Analyses

We extracted time-frequency activity for frequency bands from 1 to 40Hz, using a temporal spectral evolution method. For this procedure we first trained ICA weights on each participant's high-passed (1Hz) and segmented ([-1s 2s] relative to stimulus onset) data, to identify components related to ocular, muscular and vascular artefacts, and noisy channels. We then back projected remaining weights onto participants' raw (i.e. continuous pre-segmented) time course. We next identified where portions of this artefact-adjusted time course exceeded +/-120uv, for later removal. Time-frequency time courses were then extracted for 40 frequency values from 1 to 40 Hz. This was done by convolving each channel's fast-fourier transformed frequency spectrum with a trapezoidal digital filter of band pass width [-.5 +.5] relative to each frequency, and transition bandwidth of 1Hz. Each filtered time course was then rectified, down sampled to 125Hz, segmented ([-.2 1] relative to stimulus onset) and baseline normalised to the average value in the pre-stimulus period. We finally removed epochs if they contained portions identified pre-filtering as containing noise (>120uv).

The resulting time-frequency plots, averaged across all trial types, (see Figure 10, Panel A) show clear patterns of theta (~6Hz) activity beginning at S2 stimulus onset and peaking in the range of the N1 (170ms). We accordingly extracted specific theta time courses. This was achieved by filtering the pre-processed (using the above TSE pipeline) data to the theta (4-7Hz) band, but this time convolving the fast-fourier transformed frequency spectrum with a trapezoidal digital filter centred on 5.5Hz, with a band pass width of 3Hz and transition bandwidth of 1Hz. This filtered time course was then rectified, smoothed using a moving average (window width of 25ms), and down sampled to 125Hz. We segmented the resulting frequency time course ([-.2 1] relative to imperative stimulus onset), baseline normalised to the average value in the pre-stimulus period, and finally removed epochs if they contained portions identified pre-filtering as containing noise (>120uv).

We next tested the effect of feature (part) type and matching on the theta time course, using a factorial mass univariate procedure (fMax) similar to the Tmax procedure for pairwise comparisons. The analysis was based on a 100,000 iteration bootstrap. On each iteration we randomly reclassified trials and performed a 3x2 repeated measures ANOVA using factors Feature (Contour, Surface, Volume) and Match (Match, Mismatch) on the resulting individual averages at each data point for each channel. This created a null distribution of F-values at each time-point, for each channel, i.e., 64*400*100,000, for both main effects and the interaction effect. The same ANOVA was then conducted on individual averages of the correctly classified trials, and F-values equivalent to (or exceeding) p <.001 (one-tailed) of the null-distribution for a given time-point and channel were considered significant. Where a channel or cluster of channels exceeded a significance value for any effect, for three consecutive time-points, we submitted the channel (or central channel of the cluster) to a post-hoc tMax for all contrasts of the effect, with a one-tailed p=.001

significance criterion. We report only contrasts that reach significance at time points where the f-value for the relevant effect was also significant.

RESULTS

Behavioural Data

Overall mean accuracy was 76.69% (*SD* = 7.08). Analyses were conducted on accuracy and RTs for correct response trials. Figure 3(a) shows the mean RTs for Match and Mismatch trials as a function of feature (part) type. Figure 3(b) plots the difference scores (ms) for each participant between Contour (C) and Surface (S; C-S); and Contour (C) and Volume (V; C-S) conditions, for match and mismatch trials.

INSERT FIGURE 3(a) and 3(b) ABOUT HERE

A 2 (Match/Mismatch) x 3 Feature (Contour, Surface, Volume) repeated measures ANOVA showed only a significant main effect of Feature type, F (2, 44) = 7.01; p = .002, η^2 = 0.24. Following Leek et al (2005), separate planned analyses of the Match and Mismatch trials were conducted using one-way ANOVA. For Match trials this showed a significant effect of Feature type, F (2, 44) = 7.16, p = .002, η^2 = 0.24. There was no significant effect of Feature type for Mismatch trials (F < .1). Follow-up analyses of the Match trial data showed a significant difference in mean RTs between Contour and Volume, t (22) = 2.79, p = .01; Contour and Surface, t (22) = 2.79, p = .01; but not between Surface and Volume (t = 0.25, p =0.79). This pattern of RTs replicates the data reported by Leek et al (2005) showing an RT matching advantage for both surface and volume feature types over contours, but no advantage for volumes over surfaces.

Non-parametric analyses of response accuracy (*N* correct per condition) showed a significant difference between Match (*M* = 76.45%; *SD* = 12.38 correct) and Mismatch trials (*M* = 76.93%; *SD* = 11.42 correct) using the Wilcoxon test (p = 0.21). Friedman ANOVA on the Match condition data across Feature type was significant; *N* = 23; *d.f.* = 2; χ^2 = 18.22; p

< .001. There was also a significant difference for the Mismatch trial data; $N = 23$; *d.f.* = 2; $\chi^2 = 12.78$; $p < .001$. For Match trials, mean accuracy was higher for Surfaces $M = 82.77\%$, $SD = 8.54$) than either Volume ($M = 75.38\%$, $SD = 9.82$; T = 46.5; $Z = 2.78$; $p = .005$) or Contour feature types ($M = 69.60\%$, $SD = 14.64$; $T = 12.5$; $Z = 3.58$; $p < .001$). Accuracy for Volumes and Contours was not significantly different ($T = 65$; $Z = 1.49$; $p = .13$). The same pattern was found in Mismatch trials where mean accuracy for Surfaces ($M = 82.39\%$, $SD = 7.99$) was higher than either Contour ($M = 71.78\%$, $SD = 14\%$; $T = 36.5$; $Z = 3.08$; $p = .002$) or Volume ($M = 75\%$, $SD = 9.14$; $T = 41$; $Z = 2.95$; $p = .003$). Accuracy for Volumes and Contours was not significantly different ($T = 120.5$; $Z = 0.53$; $p = .59$). To examine whether the data showed evidence of a speed-accuracy trade-off we correlated RTs and accuracy across all conditions. The correlation ($R^2_{adjusted} = .01$) was not significant ($p > .05$) providing no evidence of a trade-off.

Analyses of ERP Data

i. Standard Waveform Analyses

P1 (70-130ms; mean peak 100ms) *- see Figure 4.* A 2 (Match/Mismatch) x 3 Feature (Contour, Surface, Volume) x Laterality (Right/Left) x Electrode repeated measures ANOVA on the amplitude data showed significant main effects of Feature F (1.87, 41.26) = 3.63, *Mse* = 12.01, $p = .038$, $\eta p^2 = 0.142$, ($\varepsilon = 0.93$); Laterality F (1.00, 22.00) = 40.24, *Mse* = 787.52, $p < .001$, $\eta p^2 = 0.64$, ($\varepsilon = 1.00$) and Electrode F (1.68, 36.98) = 10.81, *Mse* = 115.51, $p < .001$, $\eta p^2 = 0.33$, ($\varepsilon = 0.84$). There were also significant interactions of Laterality x Electrode F (1.50, 33.11) = 15.86, *Mse* = 269.05, $p < .001$, $\eta p^2 = 0.41$, ($\varepsilon = 0.75$) and Feature x Laterality x Electrode F (3.08, 67.78) = 2.78, *Mse* = 0.80, $p = .046$, $\eta p^2 = 0.11$, ($\varepsilon = 0.77$). Planned decomposition of the interaction involving the critical factor of Feature showed only a significant difference in P1 amplitude between Contour and Surface feature

types on the right hemisphere electrode cluster F (1.00, 22.00) = 4.60, Mse = 7.32, p = .04, ηp^2 = 0.17, (ε = 0.80).

INSERT FIGURE 4 ABOUT HERE

N1 (140-200ms; mean peak 170ms) *- see Figure 5.* A 2 (Match/Mismatch) x 3 Feature (Contour, Surface, Volume) x Laterality (Right/left) x Electrode repeated measures ANOVA on the amplitude data showed significant main effects of Feature F (1.50, 33.11) = 14.39, Mse = 162.02, p < .001, ηp^2 = 0.39, (ε = 0.75) and Electrode F (1.70, 37.50) = 5.03, Mse = 40.29, p = .015, ηp^2 = 0.18, (ε = 0.85). There were also significant interactions between Feature x Laterality F (1.80, 39.59) = 5.08, Mse = 19.05, p = .013, ηp^2 = 0.18, (ε = 0.90); Match x Laterality F (1.00, 22.00) = 4.26, Mse = 8.35, p = .051, ηp^2 = 0.16, (ε = 1.00) and Match x Laterality x Electrode F (1.78, 39.22) = 4.50, Mse = 0.77, p = .021, ηp^2 = 0.17, (ε = 0.89). Decomposition of the main effect of Feature showed significant differences in amplitude between Contour and Volume F (1.00, 22.00) = 9.17, Mse = 31.47, p = .006, ηp^2 = 0.29, (ε = 0.36); Contour and Surface F (1.00, 22.00) = 12.08, Mse = 30.16, p = .002, ηp^2 = 0.35, (ε = 1.00) and between Surface and Volume F (1.00, 22.00) = 17.85, Mse = 123.26, p > .001, ηp^2 = 0.44, (ε = 1.00).

We also decomposed the interaction between the critical factor of Feature and Laterality. For the left hemisphere sites there were significant differences in amplitude between Contour and Surface F (1.00, 22.00) = 5.48, Mse = 12.82, p = .029, ηp^2 = 0.19, (ε = 1.00); and between Surface and Volume F (1.00, 22.00) = 6.11, Mse = 25.80, p = .022, ηp^2 = 0.21, (ε = 1.00). In the right hemisphere there were significant differences in amplitude between Contour and Volume F (1.00, 22.00) = 14.85, Mse = 41.41, p < .001, ηp^2 = 0.40, (ε

= 1.00); Contour and Surface $F(1.00, 22.00) = 11.02$, $Mse = 17.52$, $p = .003$, $\eta p^2 = 0.33$, (ε = 1.00); and Surface and Volume $F(1.00, 22.00) = 20.59$, $Mse = 112.80$, $p < .001$, $\eta p^2 = 0.48$, (ε = 1.00). Taken together, these analyses provide evidence for differential ERP response amplitudes to the three feature types during the N1.

INSERT FIGURE 5 ABOUT HERE

P2 (220-260ms; mean peak 240ms) *- see Figure 6.* A 2 (Match/mismatch) x 3 Feature (Contour, Surface, Volume) x Laterality (Right/Midline/Left) x Electrode repeated measures ANOVA on the amplitude data showed significant main effects of Feature F (1.76, 38.83) = 7.78, $Mse = 83.50$, p = .002, $\eta p^2 = 0.26$, ($\varepsilon = 0.88$); Match F (1.00, 22.00) = 27.30, Mse = 310.96, $p < .001$, $\eta p^2 = 0.55$, ($\varepsilon = 1.00$); and Electrode F (1.00, 22.00) = 6.18, $Mse = 33.25$, p = .021, $\eta p^2 = 0.21$, ($\varepsilon = 1.00$). There were also significant interactions of Feature x Laterality F (2.37, 52.27) = 4.46, $Mse = 4.52$, $p = .012$, $\eta p^2 = 0.16$, ($\varepsilon = 0.59$); Match x Laterality F (1.83, 40.30) = 13.66, $Mse = 6.59$, $p < .001$, $\eta p^2 = 0.38$, ($\varepsilon = 0.91$); Feature x Electrode F (1.99, 43.81) = 5.02, $Mse = 0.83$, $p = .011$, $\eta p2 = 0.18$, ($\varepsilon = 0.99$); and Match x Electrode F (1.00, 22.00) = 4.91, $Mse = 0.68$, $p = .037$, $\eta p^2 = 0.18$, ($\varepsilon = 1.00$). There was also a three-way interaction of Feature x Laterality x Electrode F (2.00, 44.12) = 5.24, $Mse = 4.77$, p = .009, $\eta p^2 = 0.19$, ($\varepsilon = 0.50$). Decomposition of the interaction involving Feature x Laterality showed that for left hemisphere sites there were significant differences in mean amplitude between Contour and Surface F (1.00, 22.00) = 13.66, $Mse = 30.73$, $p = .001$, $\eta p^2 = 0.38$, (ε = 1.00) and between Surface and Volume F (1.00, 22.00) = 5.26, $Mse = 11.80$, $p = .032$, ηp^2 = 0.19, (ε = 1.000). For right hemisphere sites there were also significant amplitude differences between Contour and Surface F (1.00, 22.00) = 7.62, $Mse = 16.05$, $p = .011$, ηp^2 = 0.25, ($\varepsilon = 1.00$), and between Surface and Volume F (1.00, 22.00) = 8.95, $Mse = 21.49$, p

= .007, ηp^2 = 0.28, (ε = 1.00). For the mid-line sites there was a significant difference only between the Contour and Surface conditions F (1.00, 22.00) = 7.61, Mse = 14.93, p = .011, ηp^2 = 0.25, (ε = 1.00).

INSERT FIGURE 6 ABOUT HERE

N2 (260-320ms; mean peak 280ms) - *see Figure 7.* A 2 (Match/mismatch) x 3 Feature (Contour, Surface, Volume) x Laterality (Right/Midline/Left) x Electrode repeated measures ANOVA on the amplitude data showed significant main effects of Feature F (1.96, 43.27) = 4.16, Mse = 10.13, p = .023, ηp^2 = 0.15, (ε = 0.98); and Match F (1.00, 22.00) = 24.37, Mse = 14.71, p < .001, ηp^2 = 0.52, (ε = 1.00). There were also significant interactions of Feature x Laterality F (2.47, 54.40) = 5.50, Mse = 2.42, p = .004, ηp^2 = 0.2, (ε = 0.61); Match x Laterality F (1.70, 37.57) = 10.10, Mse = 1.76, p = .001, ηp^2 = 0.31, (ε = 0.85); Feature x Electrode F (2.28, 50.30) = 5.16, Mse = 0.55, p = .007, ηp^2 = 0.19, (ε = 0.57); and Feature x Match x Laterality F (3.13, 69.91) = 3.32, Mse = 0.88, p = .023, ηp^2 = 0.13, (ε = 0.78). Decomposition of this interaction showed significant differences for Match trials only on the left hemisphere electrodes between Contour and Surface F (1, 22) = 22.13, Mse = 2.76, p < .001, ηp^2 = 0.50, (ε = 1.0), and Volume and Surface F (1, 22) = 6.08, Mse = 3.53, p = .022, ηp^2 = 0.21, (ε = 1.0). For the right hemisphere there was a significant difference in amplitude for Match trials between Contour and Surface F (1, 22) = 5.47, Mse = 2.72, p = .029, ηp^2 = 0.19, (ε = 1.0).

INSERT FIGURE 7 ABOUT HERE

---

ii. Segmentation analysis

Topographic segmentation analysis was performed on the ERP map series for the Contour, Surface and Volume conditions in the matching condition between 50ms and 270ms after stimulus presentation to encompass the P1, N1 and P2 components and to focus on the N1. The KL criterion displayed a maximum value for four segment maps, segments that were therefore retained as best explaining the ERP series. The resulting segment maps and their periods of appearance are represented in Figure 8. An initial segment was identifiable as the P1, whilst two different segments reflected the N1. Indeed, the N1 for the Volume condition was found to be different from those of the other two conditions and was consequently termed N1v to distinguish it from the N1 in the Contour and Surface conditions. Finally, all three conditions then gave rise to the same P2 segment.

---INSERT FIGURE 8—

As indicated in the Methods section, the second step aimed to determine the statistical validity of these differences across conditions for segments N1 and N1v.

The amount of variance explained by the N1 and N1v segments were therefore measured in the three conditions of every individual's ERP map series, in the 110-210ms time window. Figure 9 represents the mean explained variance of N1 and N1v across participants in the experimental conditions.

---INSERT FIGURE 9—

Due to a non-normal distribution, the values were compared using Friedman's ANOVA. The amount of variance explained by N1 across the three conditions (Contour, Volume, Surface) revealed a statistically significant difference ($\chi^2(2) = 9.53$; p=.009; N=23). Wilcoxon's

matched pairs tests were then performed revealing that N1 better explained the map series in the Surface than the Volume condition (Z=2.91, p=.004, N=20), as well as in the Surface than Contour (Z=2.83; p=.005; N=21), while the Contour vs. Volume difference failed to reach the threshold for significance (Z=1.89; p=.058, N=18). The Friedman ANOVA was then performed on the variance explained by N1v, but this failed to reveal any significant differences ($\chi^2(2)$, = 2.17, p=.38, N=23)

iii. Time Frequency Analyses

The goal of these analyses was to examine whether the differential perceptual sensitivity to feature type that was highlighted in the previous analyses was also present in the frequency domain - potentially highlighting synchronous neural activity associated with the processing of object shape attributes. Our starting point was to compute the spatial frequency power spectra (1-40 Hz) across all conditions. Figure 10 (Panel A) shows the frequency power spectra over the P5 (left) and P6 (right) occipitotemporal channels. These showed a predominance of theta band activity around 6 Hz during the N1 component at 170ms post-stimulus onset. We consequently focussed our subsequent analysis on the theta activity. Topographical results of the fMax procedure are summarised in Figure 10 (Panel B), while Figure 10 (Panel C) depicts time courses of post-hoc tMax contrasts. For the main effect of Feature, significant f-values (with at least three consecutive significant values) were observed in the theta band over **right** occipitoparietal electrode site P6 (72-88ms; 160-176ms; 240-264ms), frontal midline site Fz (168-192ms; 248-264ms) and **right** orbitofrontal site AF4 (176-200ms; 272-288ms) - see first two rows of Figure 10 (Panel B). Post-hoc tmax contrasts (see top row, Figure 10 Panel C), collapsed across both match and mismatch trials, confirmed that theta power at channel P6 was significantly higher for both Surface and Contour relative to Volume, at 80, 160 and 168ms. In addition, theta power for Contour

significantly exceeded Volume at 240, 248, 256, 264ms, and Surface significantly exceeded Volume at 72ms. Theta power at channel Fz was significantly higher for Contour relative to Volume at 168, 176, 184, 192, 256 and 264 ms. Theta power at channel AF4 was higher for Contour relative to Volume at 176, 184, 192, 200, 272, 280 and 288ms. For the main effect of match, significant f-values (with at least three consecutive significant values) were observed in the theta band over right occipitoparietal site P6 (72-104ms; 160-192ms; 256-280ms), left orbitofrontal sites AF7 (40-56ms) and FP1 (208-232; 280-296 ms), left dorsolateral prefrontal site FC3 (160-184ms) and left posterior temporal site TP7 (288-312 ms). Post-hoc tmax contrasts (see bottom row of Figure 10 Panel C), collapsed across the three feature levels confirmed that theta power at channel P6 was significantly higher for Mismatch relative to Match trials at 80, 88, 168 and 176ms. In addition, theta power at channel AF7 was significantly higher for Match relative to Mismatch trials at 48ms. No other tMax contrasts exceeded the significance criterion, i.e., for channels FP1, FC3 or TP7. For the interaction of feature and match effects, no f-values exceeded significance thresholds at any channels for three consecutive data points, and we accordingly did not carry out any post-hoc tests.

INSERT FIGURE 10 ABOUT HERE

GENERAL DISCUSSION

The main findings were as follows: First, the behavioural data replicated the patterns reported by Leek et al (2005) showing that in match trials surfaces and volumes were processed faster than contours, but that there was no difference in RTs between surfaces and volumes. Second, in contrast, standard waveform analyses of the ERP amplitude data showed evidence for differential perceptual processing of contours, surfaces and volumes which were reliably observed over occipitoparietal electrodes from the N1 (140-200ms) component with mean peak latency of 170ms. This differential amplitude modulation was also found in posterior occipitoparietal electrodes on the later P2 (220-260ms) and N2 (260-320ms) components. Third, the topographic segmentation analysis also revealed distinct microstate patterns during the N1 reflecting the differential modulation of ERP topographies. Fourth, time frequency analyses showed predominant theta band oscillations (4-7Hz) over right occipitoparietal and orbitofrontal sites during the N1 (160-176ms). Theta activity during the N1 was modulated by feature type. Mismatch trials also showed greater right theta power over occipitoparietal sites during the N1 range.

This study yields novel insights about the early perceptual analyses of 3D object shape. In particular, they show early modulation of ERPs reflecting sensitivity to higher-order shape features comprising object surfaces and volumes within the first 200ms of stimulus processing. This provides some of the first ERP evidence that early perceptual processing during the N1 shows sensitivity to the higher-order shape structure of complex 3D objects. The results challenge theoretical models of object representation that do not attribute functional significance to higher-order surface and volumetric shape structure – a notable feature of some recent hierarchical, feedforward, multilayer image classification networks (e.g., Kheradpisheh et al., 2016; Krizhevsky et al.,2012; LeCun et al., 2015; Riesenhuber & Poggio, 1999; Serre et al., 2007). In contrast, the data support models which

explicitly contain levels of surface and/or volumetric shape structure (e.g., Biederman, 1987; Hummel & Biederman, 1992; Hummel & Stankiewicz, 1996; Leek et al., 2005; Marr & Nishihara, 1978; Reppa et al., 2009). At the same time, the data shed new light on some earlier work - including our own. Notably, our behavioural data replicated the earlier findings of Leek et al (2005). Based on a similar pattern of behavioural data, Leek et al (2005) outlined a hierarchical model of object recognition containing a level of representation of object surfaces defined by edge-bounded closed contour. Critically, in that model, higher-order surface, but not volumetric, shape structure was assumed to mediate 3D object representation. The results of current study extend those findings by showing perceptual sensitivity to both surface and volumetric structure as evidenced by the differential modulation of ERP amplitude as early as the N1. This suggests that the perceptual processing of3D object shape is sensitive to volumetric completion consistent with some structural description models of object recognition (Biederman, 1987; Hummel, 2013; Hummel & Biederman, 1992; Hummel & Stankiewicz, 1996; Marr & Nishihara, 1978). More generally, the results suggest that object representations in human vision explicitly encode, not only simple and complex edge features (as well as other shape attributes), but also higher-order geometric shape information that includes surfaces and volumetric structure. As a caveat we note that this conclusion rests on the assumption that the differential perceptual sensitivity observed here is driven by surface/volumetric shape structure and not some other critical stimulus attribute (e.g., edge and vertex distributions, bi-stability, symmetry and regularity). Additionally, it remains unclear to what extent the differential response patterns to surface and volumetric structure found in the ERP data reflect purely feedforward shape processes, or also the influence of ‘top-down’ constraints on the analysis of 3D object shape (perhaps involving stimulus-specific object knowledge

acquired as a result of stimulus repetition – e.g., see Schendan & Ganis, 2015; Schendan & Maher, 2009).

The current findings are also relevant to other recent work concerning the underlying mechanisms, neural substrates, and time course of shape information processing. For example, Oliver et al (2017) recently reported modulation of N1 amplitude during the perceptual processing of complex 3D novel objects under conditions of mono or stereo viewing. This N1 amplitude modulation was found between 145-190ms over posterior electrodes, and related to 3D object shape similarity defined in terms of either shared local volumetric part structure or global spatial configuration. This effect has been interpreted as evidence for early parallel processing of local and global object structure, consistent with other work showing early sensitivity to local and global stimulus structure in hierarchical displays within 200ms of display onset (e.g., Beaucousin et al., 2013; Han et al., 2002; Han et al., 2000; Proverbio et al., 1998). These early perceptual analyses of object structure may contribute to rapid image classification that has been reported in some studies within the first 200ms of stimulus processing (e.g., Bar, 2003; Bar et al., 2006; Cichy et al., 2014; Fabre-Thorpe, 2011; Thorpe et al., 1996; VanRullen & Thorpe, 2001).

It is also relevant to consider how the current findings relate to other ERP studies involving tasks of perceptual completion. This is relevant because our task involved the requirement to compute matches between whole objects and sub-sets of perceptually closed, but incomplete, shape information. One potentially relevant finding is the Ncl component associated with perceptual closure (e.g., Doniger et al., 2000; 2001; Sehatpour et al., 2006; Schendan & Maher, 2009; Schendan & Ganis, 2015). The Ncl refers to a bilateral occipito-temporal negativity that commences around 230ms post-stimulus onset and typically peaks around 290ms in tasks of object identification involving the presentation of degraded stimuli. Its increase correlates with identification accuracy related to decreasing levels of

image degradation. The Ncl is thought to reflect the operation of mechanisms related the recurrent processing of incomplete sensory input during object recognition (Doniger et al., 2000; 2001). Thus, whole-part perceptual completion mechanisms may be contributing to the N2 effects observed in our study between 260-320ms post-stimulus onset.

Finally, the time frequency analyses merit further discussion. These showed predominant theta band oscillations around 4-7Hz over right occipitoparietal electrode P6 (72-88ms; 160-176ms; 240-264ms), frontal midline site Fz (168-192ms; 248-264ms) and right orbitofrontal site AF4 (176-200ms; 272-288ms). Mismatch trials also showed greater theta power over right occipitoparietal sites during the N1, while left orbitofrontal sites also showed higher theta power for match trials in an earlier window (48ms). In other work, alpha band activity, possibly related to perceptual integration, has previously been associated with object recognition (e.g., Bar, 2003; Bar et al., 2006; Mima et al., 2001). For example, Bar et al (2006) have shown, using MEG, orbitofrontal alpha activity phase-locked with occipital cortex around 80ms and with temporal-fusiform areas around 130-180ms post-stimulus onset during object recognition. These findings were used to support a model of object recognition involving early, top-down, low-spatial frequency orbitofrontal modulation of occipitotemporal ventral stream processing. Our finding of predominant theta band activity over the same network is novel in this context. Elsewhere, in other work, theta band oscillations have also been linked with short-term memory via modulation of gamma (30-80 Hz) activity (e.g., Basar et al., 2001; Demiralp et al., 2007) and long-range synchronisation during working memory retention (e.g., von Stein & Sarnthein, 2000). In the present context the predominance of theta activity may relate to memory requirements of the task as observers had to retain a representation of the whole (S1) object during matching to the feature (S2) part stimulus. However, it remains of relevance that this theta band modulation interacted with feature type - providing converging evidence that perceptual-

memory mechanisms differentially process object shape information. Further work is needed to fully elucidate the functional significance of this theta band activity in relation to early perceptual analyses of 3D object shape properties.

In summary, this study used event-related potentials (ERPs) to investigate early perceptual processing of three-dimensional (3D) object shape. Observers performed a whole-part object matching task. Part match stimuli comprised regions of closed edge contour, surfaces or volumetric primitives. The behavioural data showed that surface and volumetric primitives were processed faster than contours, but there was no difference in response latency between surfaces and volumes - replicating an earlier study by Leek et al (2005). ERPs were analysed using a convergence of approaches based on stimulus dependent amplitude modulations of evoked potentials, topographic segmentation and spatial frequency oscillations. The results showed differential perceptual processing of contours, surface and volumetric part stimuli. This was first reliably observed over occipitoparietal electrodes during the N1 (140-200ms) with a mean peak latency of 170ms, and continued on subsequent P2 (220-260ms) and N2 (260-320ms) components. Topographic segmentation analyses showed distinct microstate patterns that distinguished among part feature types also during the N1. Analyses of spatial frequency oscillations showed predominant theta band activity, modulated by part feature type, around 4-7Hz over right occipitoparietal and orbitofrontal sites during the N1. These findings yield novel insights into the early perceptual processing of 3D object shape. In particular, they show early sensitivity to higher-order shape structure within the first 200ms of stimulus processing. The results challenge theoretical models of object recognition that do not attribute functional significance to higher-order 3D shape structure during visual perception.

Acknowledgements

This study was supported by grants from the Economic and Social Research Council (ESRC: RES-062-23-2075), Experimental Psychology Society (EPS), British Academy, Royal Society and Wales Institute of Cognitive Neuroscience to E.C.L.

Competing Interest Statement

The authors declare that they have no competing interests.

Data Sharing Statement

All data sets reported in this study are freely available from the corresponding author on request.

REFERENCES

Arguin, M. & Leek, E.C. (2003). Orientation-dependence in visual object recognition: Further evidence from repetition priming and picture naming. *Perception & Psychophysics*, **65**, 469-477.

Bar, M. (2003). A cortical mechanism for triggering top-down facilitation in visual object identification. *Journal of Cognitive Neuroscience, **15***, 600-609.

Bar, M., Kassam, K.S., Ghuman, A.S., Boshyan, J, Schmid, A.M., Dale, A.M., Hamalainen, M.S., Marinkovic, K., Schacter, D.L., Rosen, B.R. & Halgren, E. (2006). Top-down facilitation of visual recognition. *Proceedings of the National Academy of Sciences, **103***, 449-454.

Basar, E., Basar-Eroglu, C., Karakas, S. & Schumann, (2001). M. Gamma, alpha, delta and theta oscillations govern cognitive processes. *International Journal of Psychophysiology, **39***, 241-248.

Beaucousin, V., Simon, G., Cassotti, M., Pineau, A., Houdé, O. & Poirel, N (2013). Global interference during early visual processing: ERP evidence from a rapid global/local selection task. *Frontier in Psychology, **4***, 1-6: doi: 10.3389/fpsyg.2013.00539

Brandeis D. & Lehmann D. (1986) Event-related potentials of the brain and cognitive processes: approaches and applications. *Neuropsychologia **24***(1):151-168

Brunet, D., Murray, M. M., and Michel, C. M. (2011). Spatiotemporal analysis of multichannel EEG: CARTOOL. *Computational Intelligence and Neuroscience*, 813870. doi: 10.1155/2011/813870

Carandini, M., Demb, J.B., Mante, V., Tolhurst, D.J., Dan, Y., Olshausen, B.A. et al. (2005). Do we know what the early visual system does? Journal of Neuroscience, **25**, 10577-10597.

Cichy, R.M., Pantazis, D. & Oliva, A. (2014). Resolving human object recognition in space and time. *Nature Neuroscience, **17***, 455-462.

Cristino, F., Davitt, L., Hayward, W. & Leek, E.C. (2015). Viewpoint interpolation during object recognition is depth blind: Evidence from stereoscopic presentation. *Quarterly Journal of Experimental Psychology, **68**, 2419-2436.*

Demiralp, T., Bayraktaroglu, Z., Lenz, D., Junge, S. Busch, N.A., Maess, B., Ergen, M., Herrmann, C.S. (2007). Gamma amplitudes are coupled to theta phase in human EEG during visual perception. International *Journal of Psychophysiology, **64***, 24-30.

Doniger, G.M., Foxe, J.J., Schroeder, C.E., Murray, M.M., Higgins, B.A. & Javitt, D.C. (2001). Visual perceptual learning in human object recognition areas: A repetition priming study using high-density electrical mapping. *NeuroImage, **13***, 305-313.

Doniger, G.M., Foxe, J.J., Murray, M.M., Higgins, B.A., Snodgrass, J.G., Schroeder, C.E. & Javitt, D.C. (2000). Activation time course of ventral visual stream object recognition areas: High density electrical mapping of perceptual closure processes. *Journal of Cognitive Neuroscience, **12***, 615-621.

Fabre-Thorpe, M. (2011). The characteristics and limits of rapid visual categorization. *Frontiers in Psychology, **2***, 1-12.

Flevaris, A.V., Martinez, A. & Hillyard, S.A. (2013). Neural substrates of perceptual integration during bistable object perception. *Journal of Vision, **13*** (17), 1-25.

Gratton, G., Coles, M.G. & Donchin, E. (1983). A new method for off-line removal of ocular artifact. *Electroencephalography and Clinical Neurophysiology, **55***(4):468-84.

Han, S., Weaver, J.A., Murray, S.O., Kang, X., Yund, E.W. & Woods, D.L. (2002). Hemispheric asymmetry in global/local processing: Effects of stimulus position and spatial frequency. *Neuroimage, **17***, 1290-1299.

Han, S., He, X. & Woods, D.L. (2000). Hierarchical processing and level-repetition effect as indexed by early brain potentials. *Psychophysiology, **37***, 817-830.

Harris, I., Dux, P. E., Benito, C. T. & Leek, E. C. (2008). Orientation sensitivity at different stages of object processing: Evidence from repetition priming and naming. *PLoS ONE, **3** (5),* e2256. doi: 10.1371/journal.pone.0002256

Hubel, D.H. & Wiesel, T.N. (1962). Receptive fields and functional architecture in two nonstriate visual areas (18 and 19) of the cat. *Journal of Neurophysiology, **28***, 229-289.

Hummel, J.E. (2013). Object recognition. In D. Reisburg (Ed.). *Oxford Handbook of Cognitive Psychology*. pp 32-46. Oxford. Oxford University Press.

Hummel, J. E., & Stankiewicz, B. J. (1996). An architecture for rapid, hierarchical structural description. In T. Inui & J. McCelland (Eds.), *Attention and Performance XVI: On information integration in perception and communication* (pp.93-121). Cambridge, MA: MIT Press.

Kheradpisheh, S.R, Ghodrati, M., Ganjtabesh, M. & Masquelier, T. (2016). Deep networks can resemble human feed-forward vision in invariant object recognition. *Scientific Reports, **6***, 32672. doi: 10.1038/srep32672

Krizhevsky, A., Sutskever, I. & Hinton, G. Imagenet classification with deep convolutional neural networks. In *Neural Information Processing Systems (NIPS)*, 1–9 (2012).

Kubulius, J., Wagemans, J. & Op de Beeck, H.P. (2014). A conceptual framework of computations in mid-level vision. *Frontiers in Computational Neuroscience*, doi: 10.3389/fncom.2014.00158.

LeCun, Y., Bengio, Y., & Hinton, G. (2015). Deep learning. *Nature, 521*, 436 – 444.

Leek, E.C. (1998a). The analysis of orientation dependent time costs in visual recognition. *Perception, **27***, 803-816.

Leek, E.C. (1998b). Effects of stimulus orientation on the recognition of common poly-oriented objects. *Psychonomic Bulletin and Review **5***, 650-658.

Leek, E.C., Roberts, M., Oliver, Z., Cristino, F. & Pegna, A. (2016). Early differential sensitivity of evoked-potentials to local and global shape during the perception of three-dimensional objects. *Neuropsychologia, **89***, 495-509.

Leek, E.C., Reppa, I., Rodiguez, E. & Arguin, M. (2009). Surface but not volumetric part structure mediates three-dimensional shape representation. *Quarterly Journal of Experimental Psychology, **62**,* 814-829.

Leek, E.C., Atherton, C.J. & Thierry, G. (2007). Computational mechanisms of object constancy for visual recognition revealed by event-related potentials. *Vision Research, **5***, 706-713.

Leek, E.C., Reppa, I. & Arguin, M. (2005). The structure of 3D object shape representations: Evidence from part-whole matching. *Journal of Experimental Psychology: Human Perception and Performance*, ***31***, 668-684.

Lehmann D. (1987). Principles of spatial analysis, In: A.S. Gevins, A. Remond (Eds.), Methods of Analysis of Brain Electrical and Magnetic Signals, *Handbook of Electroencephalography and Clinical Neurophysiology*, Vol. 1, Elsevier, Amsterdam, pp. 309–354.

Lehmann D, Pascual-Marqui R.D. & Michel C.M. (2009) EEG microstates. *Scholarpedia* **4**(3):7632

Lehmann D, Skrandies W. (1984) Spatial analysis of evoked potentials in man – A review. *Progress in Neurobiology, **23***:227-250

Lloyd-Jones T.J., Roberts M.V., Leek E.C., Fouquet N.C. & Truchanowicz E.G. (2012) The time course of activation of object shape and shape+colour representations during memory retrieval. *PLoS ONE7*(11): e48550. https://doi.org/10.1371/journal.pone.0048550

Luck, S. J. & Gaspelin, N. (2017), How to get statistically significant effects in any ERP experiment (and why you shouldn't). Psychophysiology, **54**: 146–157. doi:10.1111/psyp.12639

Michel C.M., Seeck M., Landis T. (1999) Spatiotemporal dynamics of human cognition. News *Physiological Sciences*, **14**:206-214

Mima, T., Oluwatimilehin, T., Hiraoka, T. & Hallet, M. (2001). Transient interhemispheric neuronal synchrony correlates with object recognition. *Journal of Neuroscience*, **1**:21 (11), 3942-3948.

Murray MM, Brunet D, Michel CM (2008) Topographic ERP analyses: A step-by-step tutorial review. *Brain Topography*, **20**:249-264

Oliver, Z.J., Cristino, F., Roberts, M.V., Pegna, A.J. & Leek, E.C. (2018). Stereo viewing modulates three-dimensional shape processing during object recognition: A high-density ERP study. *Journal of Experimental Psychology: Human Perception and Performance*, **44** (4), 518-534. doi: 10.1037/xhp0000444

Pasupathy, A. & Connor, C.E. (2001). Shape representation in area V4 of the macaque: Position-specific tuning for boundary confirmation. *Journal of Neurophysiology, **86***, 2505-2519.

Pegna, A., Darque, A., Roberts, M.V. & Leek, E.C. (2018). Effects of stereo disparity on early-evoked potentials associated with the classification of three-dimensional object shape. *Quarterly Journal of Experimental Psychology*, **71** (6), 1419-1430.

Picton, T.W., , S., Berg P., Donchin, E., Hillyard, S.A., Johnson, R. Jr, Miller, G.A. , Ritter, W., Ruchkin, D.S., Rugg, M.D. & Taylor, M.J. (2000). Guidelines for using human event-related potentials to study cognition: recording standards and publication criteria. *Psychophysiology, **37*** (2), 127-152.

Pizlo, Z. (2008). *3D Shape: Its unique place in visual perception*. MIT Press. Cambridge. MA.

Proverbio, A.M., Minniti, A. & Zani, A. (1998). Electrophysiological evidence of a perceptual precedence of global vs. local visual information. *Brain Research, **6***, 321-334.

Riesenhuber, M., & Poggio, T. (1999). Hierarchical models of object recognition in cortex. *Nature Neuroscience, **2(11),*** 1019–1025. doi:10.1038/14819

Reppa, I., Greville, W.J. & Leek, E.C. (2015). The role of surface-based representations of shape in visual object recognition. *Quarterly Journal of Experimental Psychology, **68**, 2351-2369.*

Schendan, H.E., & Kutas, M. (2007). Neurophysiological evidence for the time course of activation of global shape, part and local contour representations during visual object categorisation and memory. *Journal of Cognitive Neuroscience, **19***, 734-749.

Schendan, H.E., & Maher, S.M. (2009). Object knowledge during entry-level categorisation is activated and modified by implicit memory after 200ms. *Neuroimage, **44***, 1423-1438.

Schendan, H.E., & Ganis, G. (2015). Top-down modulation of visual processing and knowledge after 250ms supports object constancy of category decisions. *Frontiers in Psychology, **6***, 1289. doi:10.3389/fpsyg.2015.01289

Serre, T., Oliva, A. & Poggio, T. (2007). A feedforward architecture accounts for rapid categorization. *Proceedings of the National Academy of Sciences, **104***, 6424-6429.

Sehatpour, P., Molholm, S., Javitt, D.C. & Foxe, J.J. (2006). Spatiotemporal dynamics of human object recognition processing: An integrated high-density electrical mapping and functional imaging study of "closure" processes. *NeuroImage, **29***, 605-618.

Stein, A. & Sarnthein, J. (2000). Different frequencies for different scale of cortical integration: from local gamma to long range alpha/theta synchronization. *International Journal of Psychophysiology, **38***, 301-313.

Tarr, M. J., & Bulthoff, H. H. (1998). *Object recognition in man, monkey, and machine.* MIT Press, Cambridge, MA.

Thorpe, S.J., Fize, D. & Marlot, C. (1996). Speed of processing in the human visual system. *Nature, **381***, 520-522.

Tibshirani R, Walther G, Botstein D, Brown P. (2005) Cluster validation by prediction strength. *Journal of Computational and Graphical Statistics*, **14**:5: 11–28

VanRullen, R., & Thorpe, S. J. (2001). The time course of visual processing: from early perception to decision-making. *Journal of Cognitive Neuroscience, **13**(4),* 454-461. doi:10.1162/08989290152001880

Vaughan H.G. Jr (1982). The neural origins of human event-related potentials. *Annals of the New York Academy of Sciences, **388***:125-138

FIGURE LEGENDS

Fig 1. The stimulus set used in the current study. Each object (N=12) is shown along with its corresponding matching feature (Contour, Surface, Volume) stimuli.

Fig 2. Illustration of the trial procedure (based on Leek et al., 2005 - Exp 3).

Fig 3. (a) Mean RTs (ms) as a function of feature type (Contour, Surface and Volume) for (correct) match and mismatch trials. Bars show standard error of the mean. **(b)** Difference scores (ms) for Contour (C) versus Surface (S; C-S) and Contour versus Volume (V; C-V) conditions across participants in the match and mismatch trials.

Fig 4. Grand average (match) waveforms (left) and topographies (right) for the **P1** component (70-130ms - highlighted mean peak 100ms) across conditions at electrodes P07 (left hemisphere) and P08 (right hemisphere).

Fig 5. Grand average (match) waveforms (left) and topographies (right) for the **N1** component (140-200ms – highlighted mean peak 170ms) across conditions at electrodes P5 (left hemisphere) and P6 (right hemisphere).

Fig 6 Grand average (match) waveforms (left) and topographies (right) for the **P2** component (220-260ms – highlighted mean peak 240ms) across conditions at electrodes P3 (left hemisphere) and P4 (right hemisphere).

Fig 7. Grand average (match) waveforms (left) and topographies (right) for the **N2** component (260-320ms – highlighted mean peak 280ms) across conditions at electrodes P3 (left hemisphere), Pz (midline) and P4 (right hemisphere).

Fig 8. Results of topographic segmentation of grand average ERPs. A. Grand average ERPs of the matching condition on the 3 conditions are shown for Contour, Surface and Volume, respectively from left to right, with all electrode traces superimposed (inset lower right indicates voltage and time). The vertical grey lines situated on the traces mark the time of stimulus presentation (time 0). Overlaid coloured boxes indicate the time of occurrence of the maps identified in the topographic segmentation. Blue box indicates presence of P1 and black box indicates presence of P2 in the grand averages. The N1 in the volume condition (N1v in brown) differed from the N1 in the other two conditions (N1 in green). B. The map topographies are shown for P1, N1, N1v and P2 (blue, green, brown and black respectively) on a schematised scalp seen from above (forehead on top, left ear on the left). Red regions indicate positive, and blue areas negative regions (see inset on the right).

Fig 9. Amount of variance explained by maps N1 and N1v. The amount of variance (y axis) explained by maps N1 (green) and N1v (brown) during the N1 time period is displayed as a function of experimental condition

Fig 10 Panel A - Event related spectral activity for channel P5 and P6 relative to imperative stimulus onset (time 0; thick black line) for frequency bands from 1 to 40Hz. Spectral activity in each band is extracted using the TSE method (unsmoothed) and normalised to pre-stimulus period. Spikes of activity in the theta band (~6Hz) appear to peak during N1 range (170ms; dashed red line) in both channels, more prominently on the right. Panel B - Topographies from n=100,000 fMax permutation test, for main effects of feature and match on theta (4-7Hz) time courses. Values beneath each topography are latencies, relative to imperative stimulus onset (ms). Topographies show effects of feature on theta power, across right occipitoparietal (OPC: 72-88ms; 160-176ms; 240-264ms), frontal midline (168-192ms; 248-264ms) and right orbitofrontal (OFC: 176-200ms; 272-288ms) sites and effects of match over right OPC site (72-96ms; 160-192ms; 256-280ms), left OFC sites (40-56ms; 208-232; 280-296 ms), and left dorsolateral prefrontal sites (DLPFC: 160-184ms). Panel C - Theta timecourse contrasts. Shaded pink areas display data points where relevant main effect was significant at that channel, while */** display data points where relevant post-hoc tMax contrast was significant. Note that tMax contrasts were only carried out for data points where relevant main effect was significant in the fMax test. Top row shows theta time courses for contour (red), surface (green) and volume (blue) trials, collapsed across match and mismatch, at channels P6 (left), Fz (centre) and AF4 (right). Significantly more right OPC theta power is observed for both surface and contour trials, relative to volume, at a range of data points in the N1 range. Theta power was also significantly higher at frontal sites for contour, relative to volume trials in the N1 range. Bottom row shows theta time courses for match (solid) and mismatch (dashed) trials, collapsed across all feature types, at channels P6 and AF7. Mismatch trials show greater right OPC theta power in the N1 range, while left OFC theta power is significantly higher for match trials in an earlier window (48ms).

FIGURE 1

FIGURE 1 (cont)

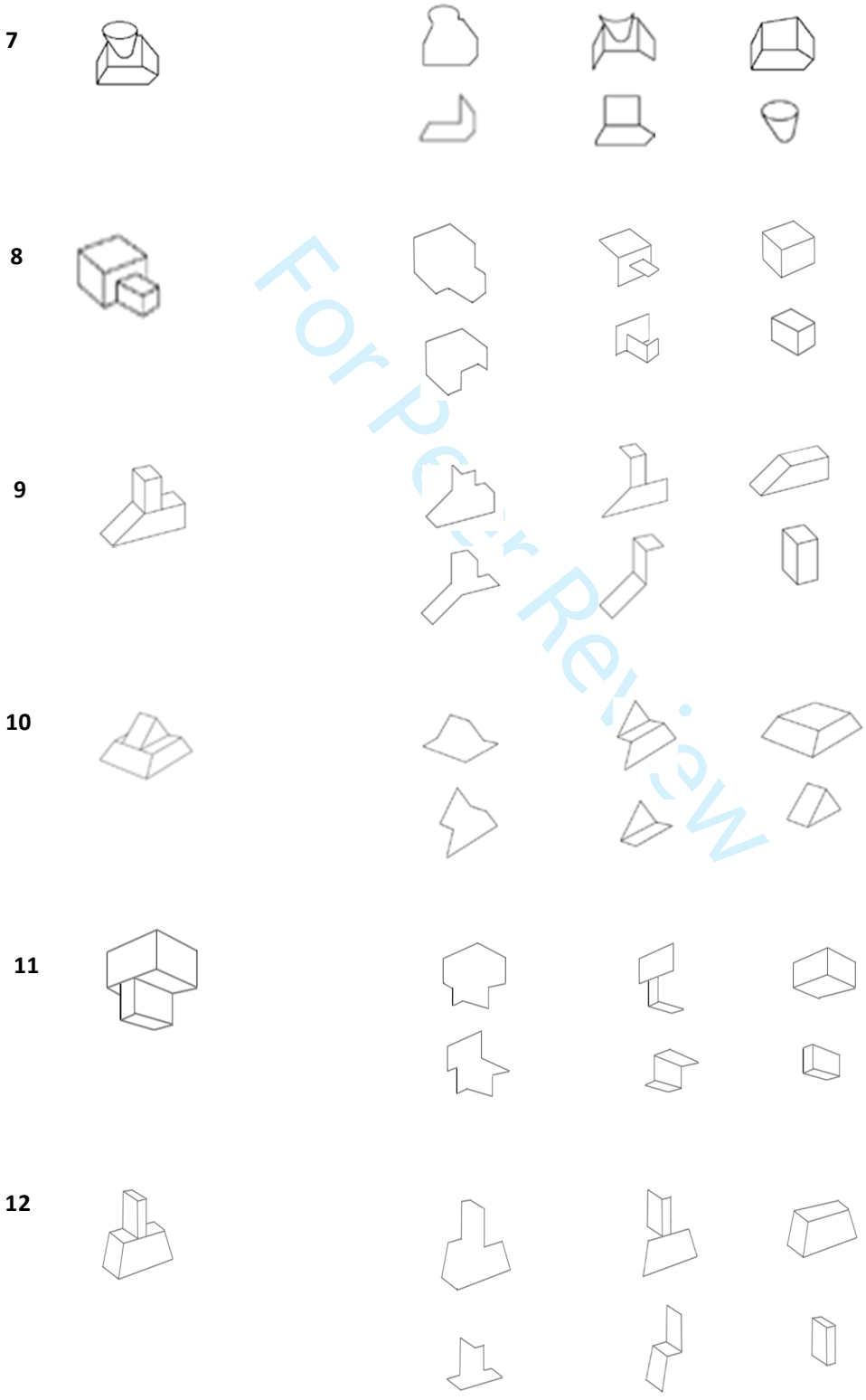

FIGURE 2

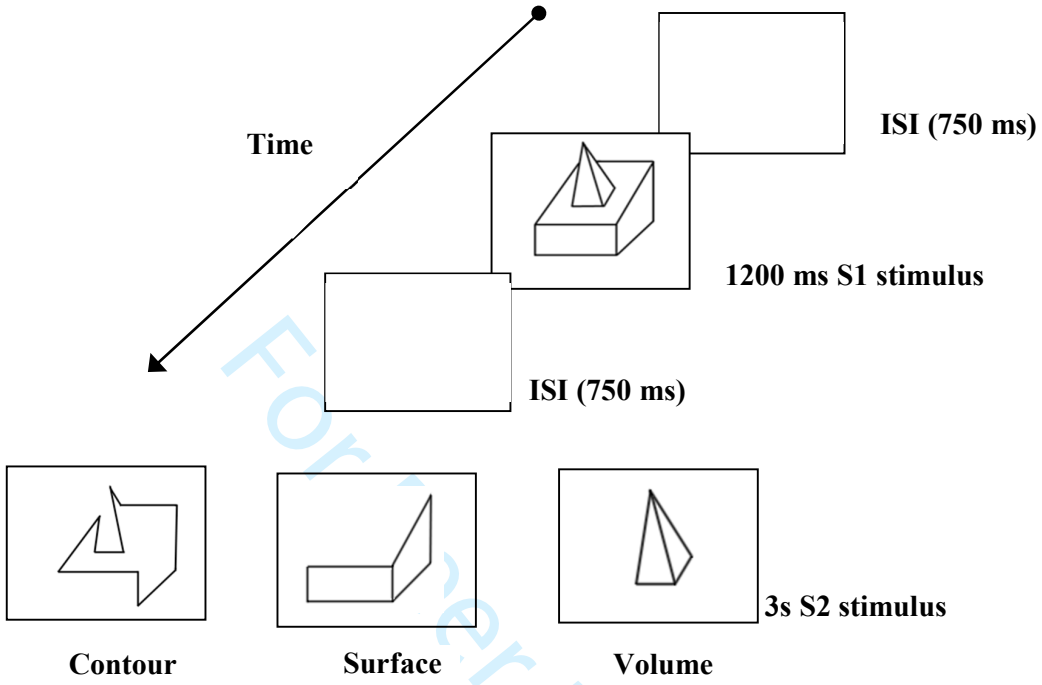

FIGURE 3a

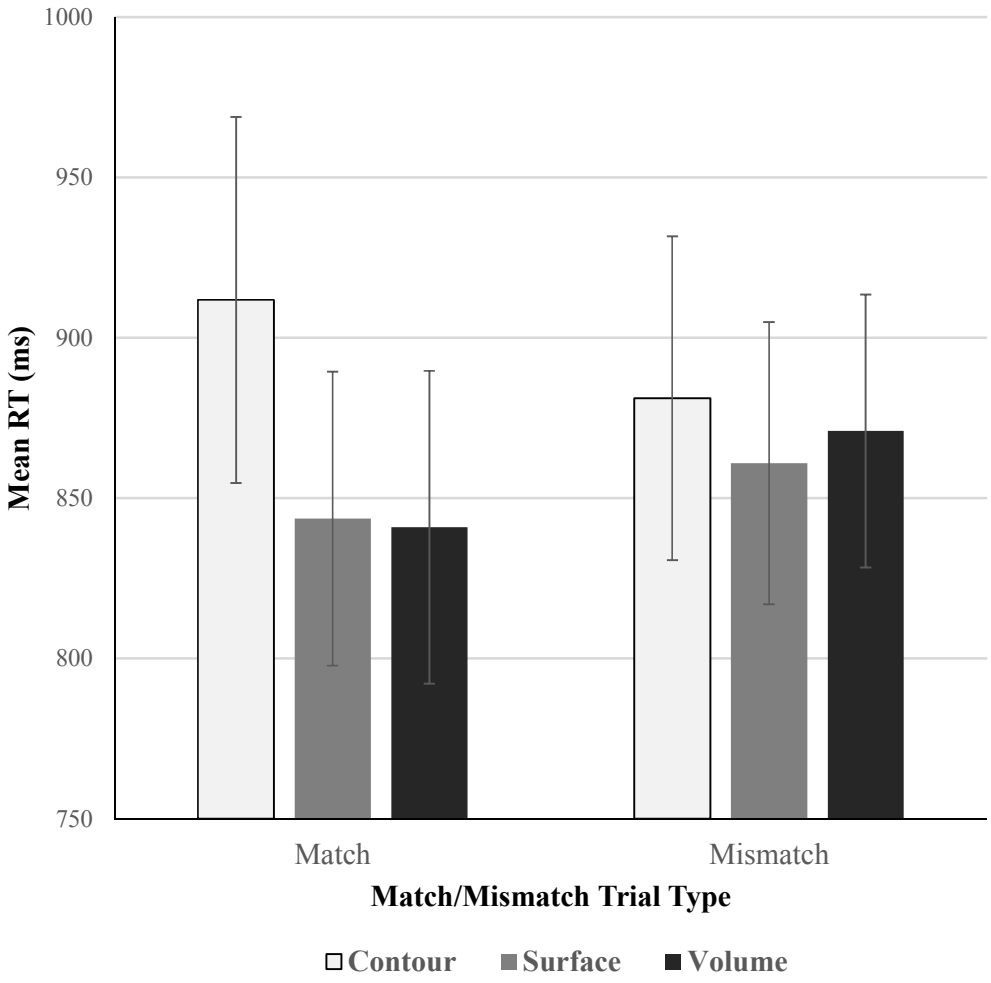
1000
950
900
850
800
750
Mean RT (ms)
Match
Mismatch
Match/Mismatch Trial Type
Contour
Surface
Volume

FIGURE 3b

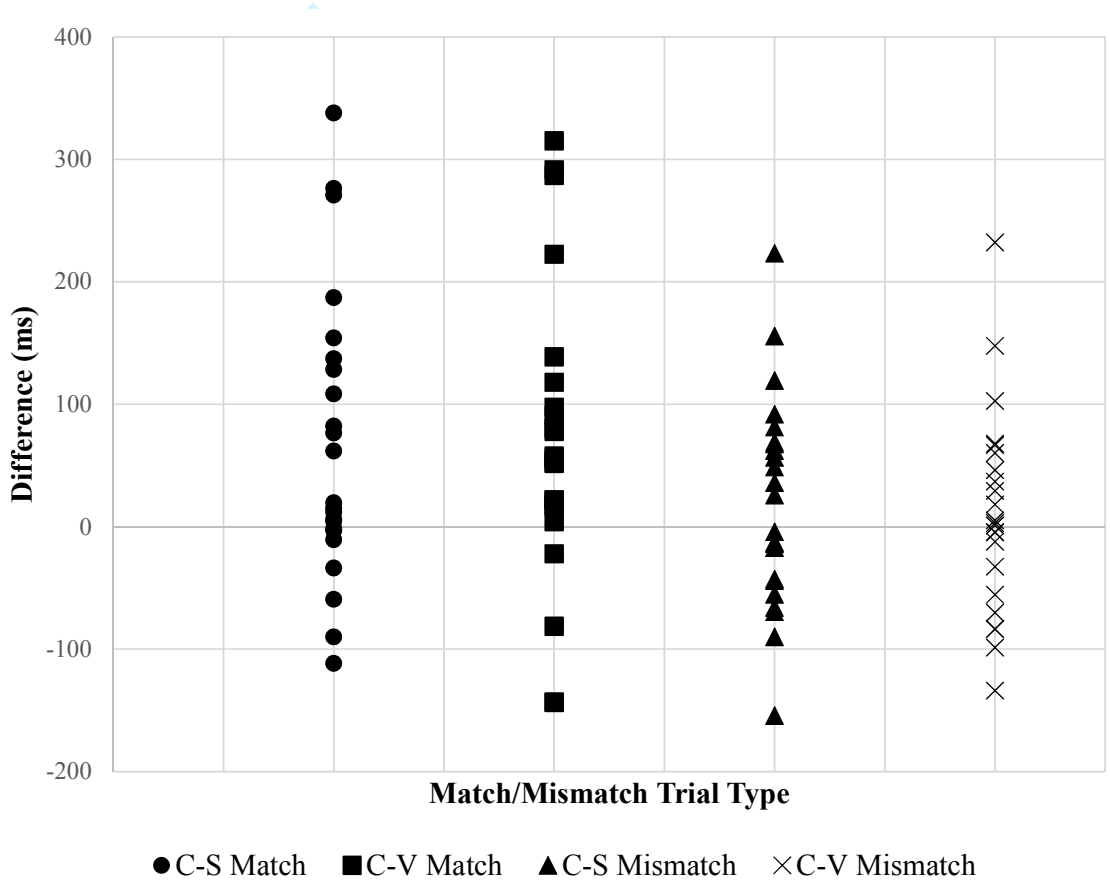
400
300
200
100
0
-100
-200
Difference (ms)
Match/Mismatch Trial Type
C-S Match
C-V Match
C-S Mismatch
C-V Mismatch

FIGURE 4

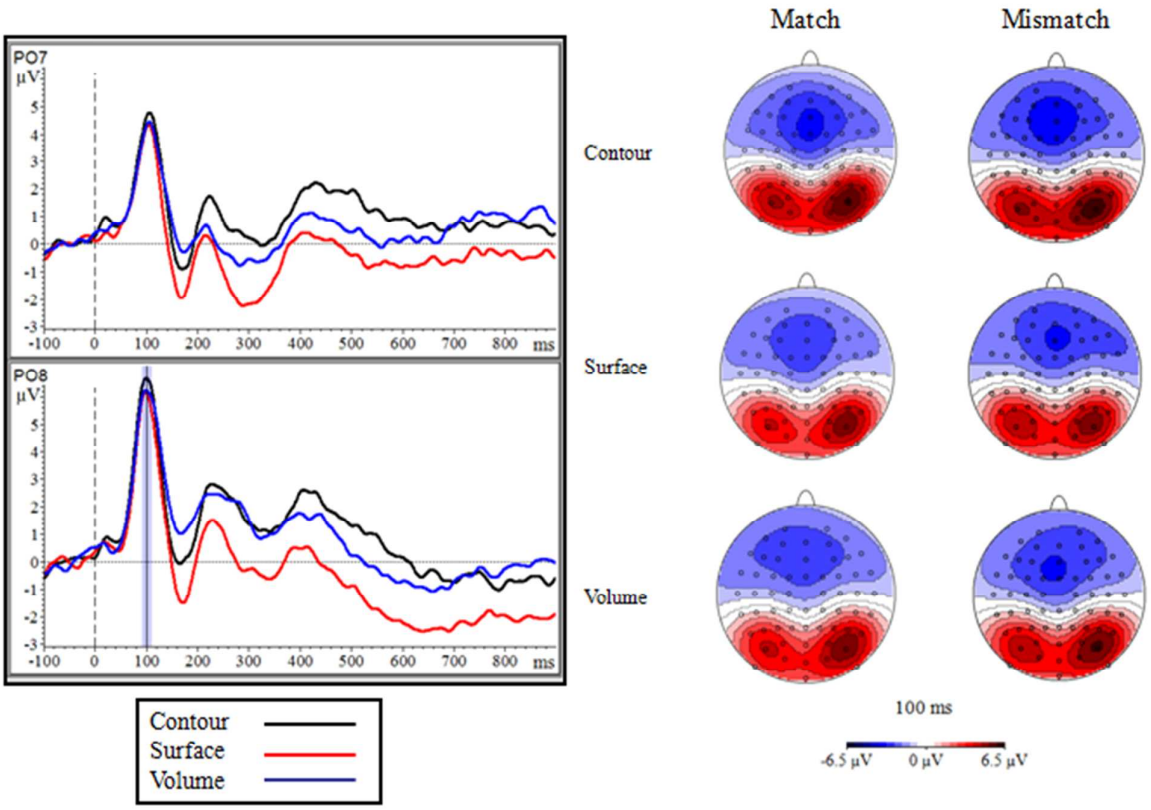
PO7
µV
PO8
µV
-100 0 100 200 300 400 500 600 700 800 ms
Contour
Surface
Volume
Match
Mismatch
Contour
Surface
Volume
100 ms
-6.5 µV 0 µV 6.5 µV

FIGURE 5

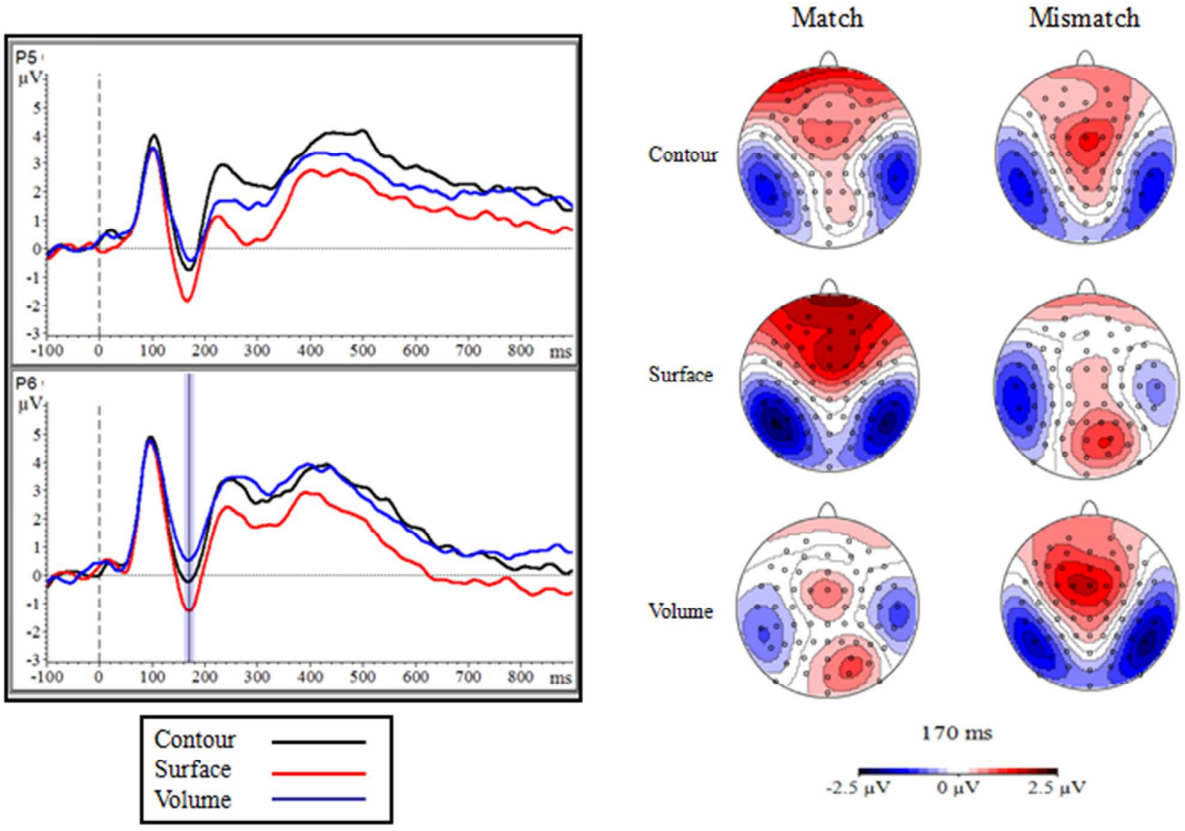
P5
µV
P6
µV
-100 0 100 200 300 400 500 600 700 800 ms
Contour
Surface
Volume
Match
Mismatch
Contour
Surface
Volume
170 ms
-2.5 µV
0 µV
2.5 µV

FIGURE 6

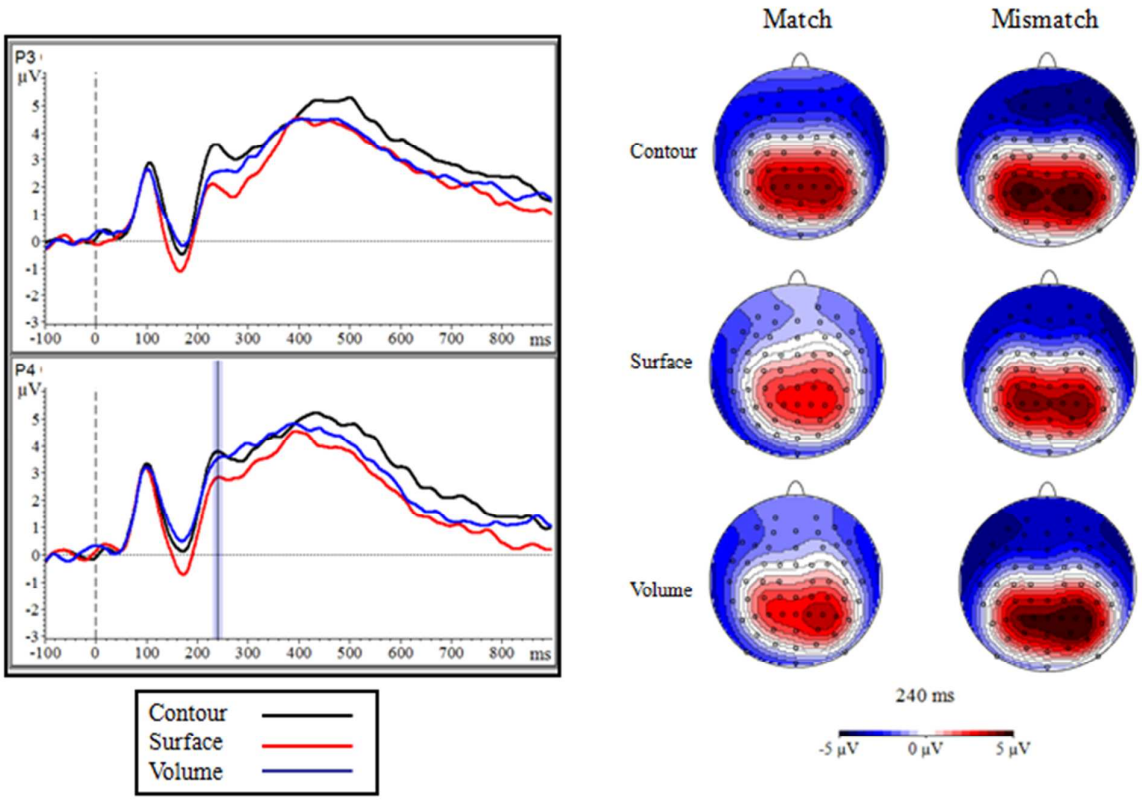
P3
µV
P4
µV
-100 0 100 200 300 400 500 600 700 800 ms
Contour
Surface
Volume
Match
Mismatch
Contour
Surface
Volume
240 ms
-5 µV
0 µV
5 µV

FIGURE 7

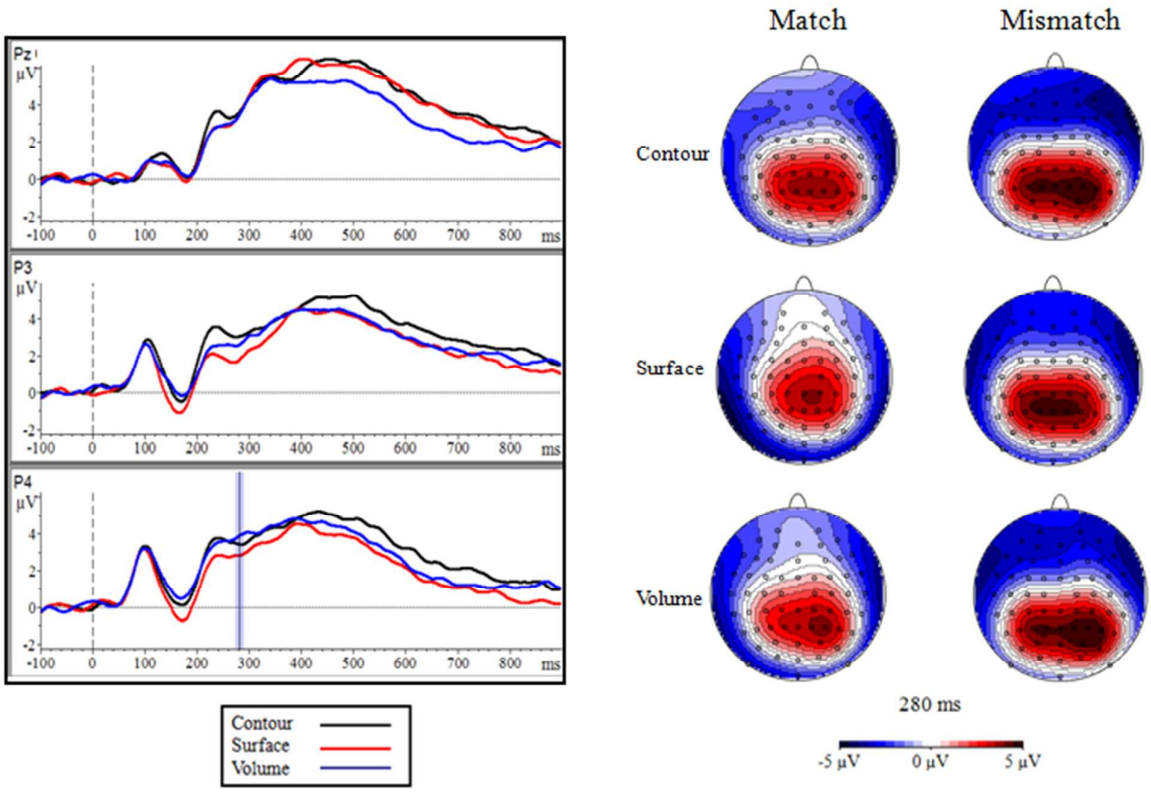

FIGURE 8

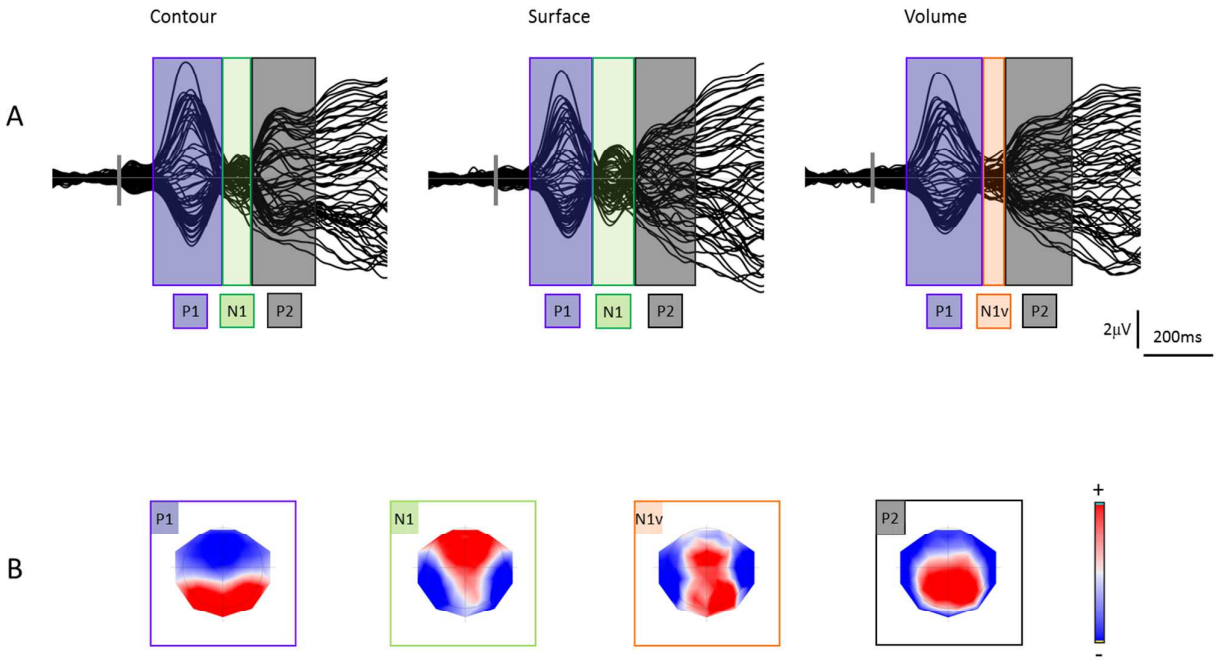

FIGURE 9

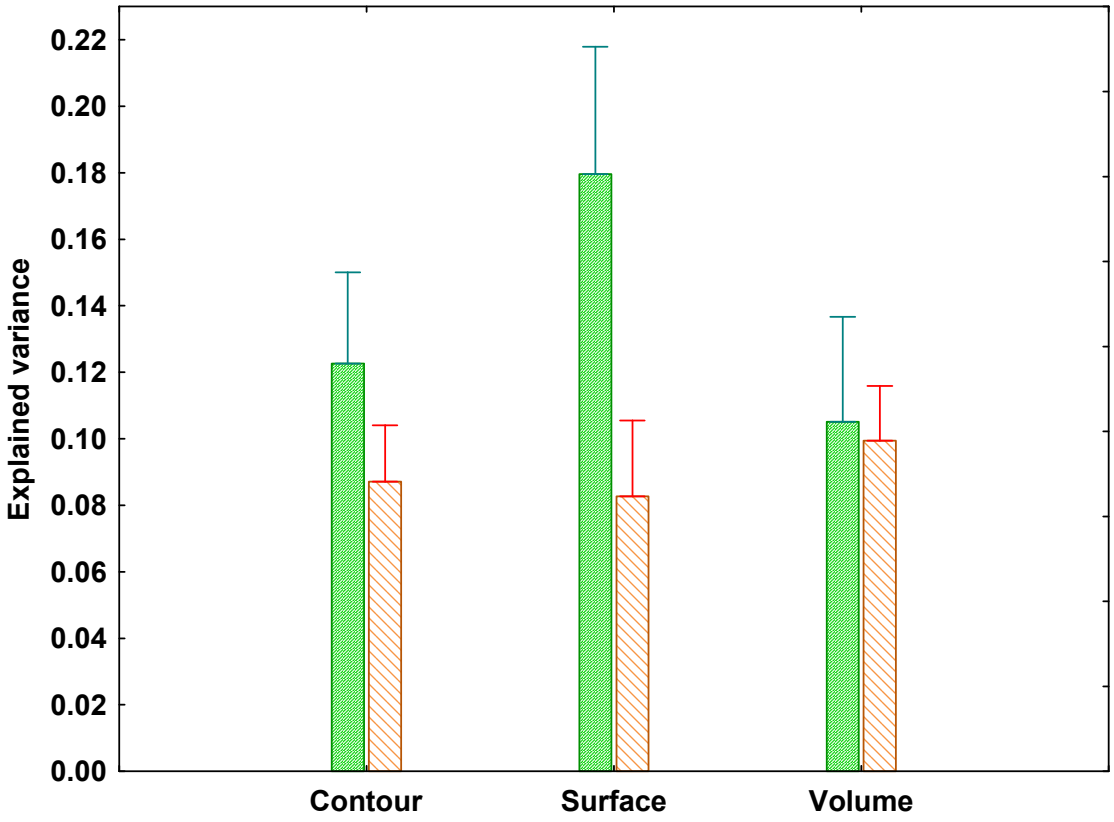
Explained variance
0.22
0.20
0.18
0.16
0.14
0.12
0.10
0.08
0.06
0.04
0.02
0.00
Contour
Surface
Volume

FIGURE 10

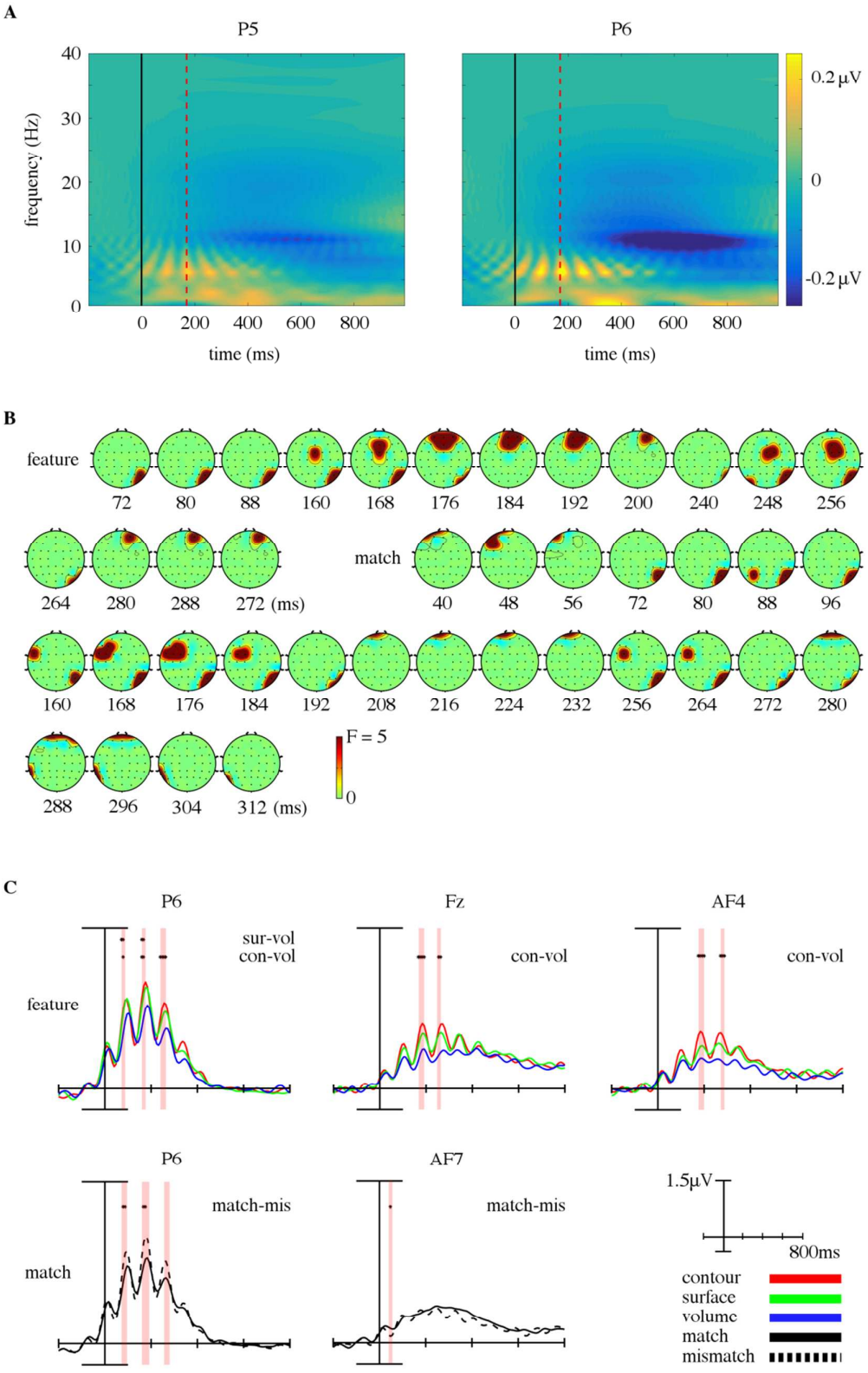
A
P5
P6
frequency (Hz)
40
30
20
10
0
0 200 400 600 800
time (ms)
0.2 µV
0
-0.2 µV
B
feature
72 80 88 160 168 176 184 192 200 240 248 256
264 280 288 272 (ms)
match
40 48 56 72 80 88 96
160 168 176 184 192 208 216 224 232 256 264 272 280
288 296 304 312 (ms)
F = 5
0
C
P6
sur-vol
con-vol
feature
Fz
con-vol
AF4
con-vol
P6
match-mis
match
AF7
match-mis
1.5µV
800ms
contour
surface
volume
match
mismatch

FIGURE 1

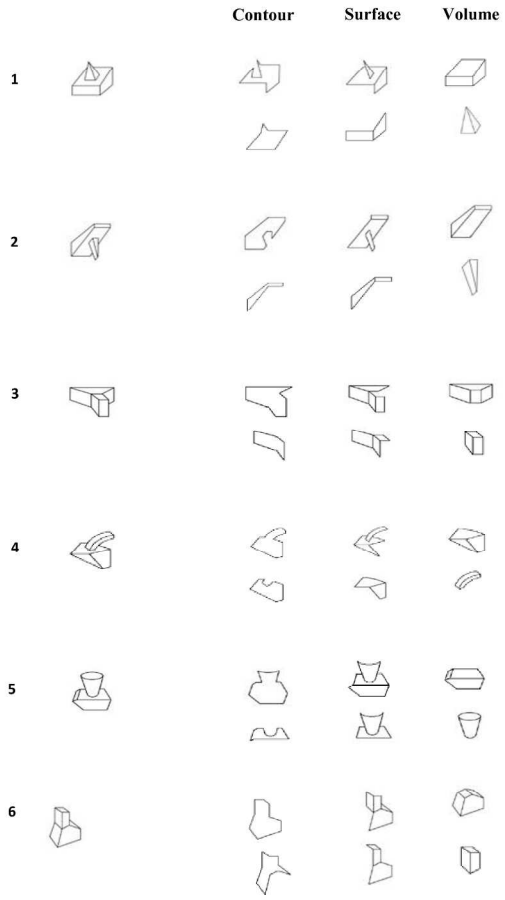

Figure 1_1

210x297mm (300 x 300 DPI)

FIGURE 1 (cont)

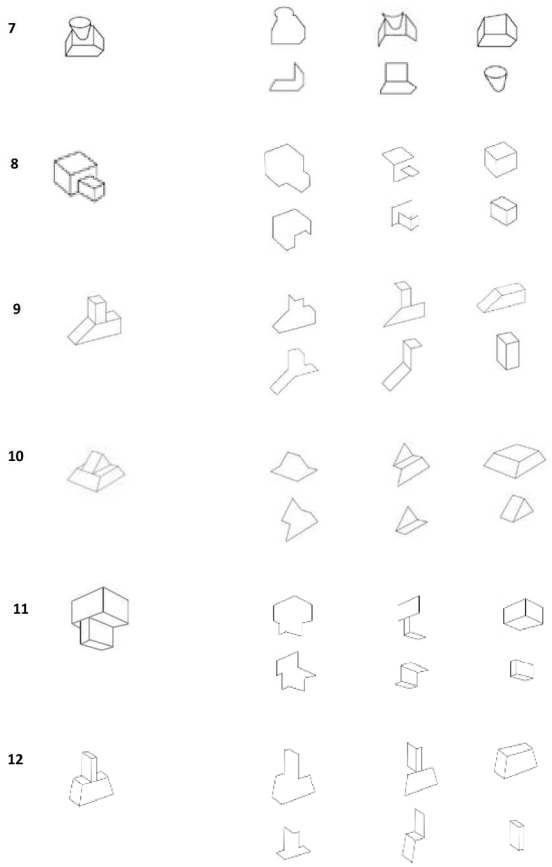

Figure 1_2

210x297mm (300 x 300 DPI)

FIGURE 2

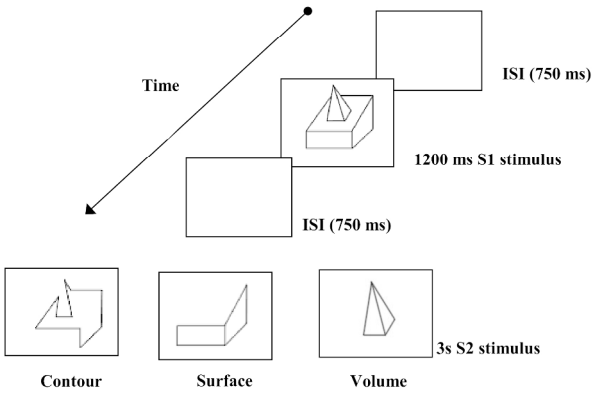

Figure 2

210x297mm (300 x 300 DPI)

FIGURE 3a

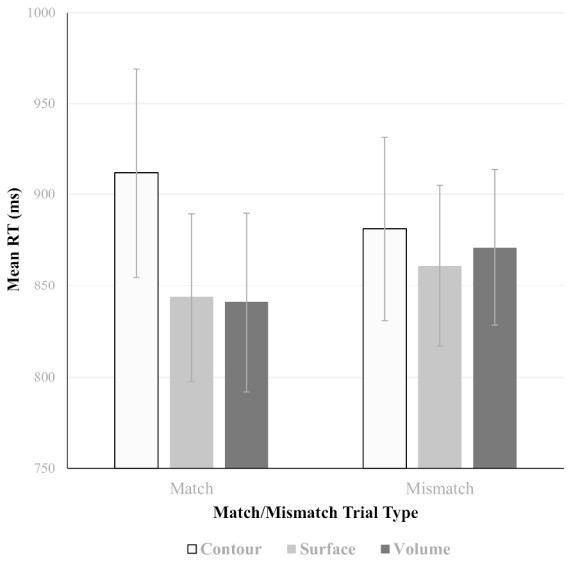

Figure 3a

210x297mm (300 x 300 DPI)

FIGURE 3b

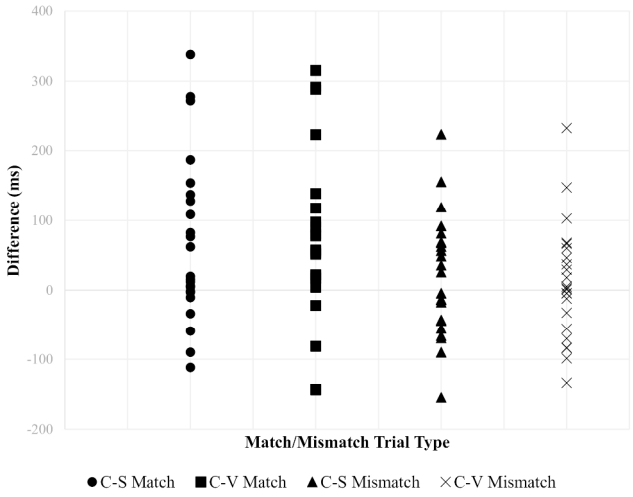

Figure 3b

210x297mm (300 x 300 DPI)

FIGURE 4

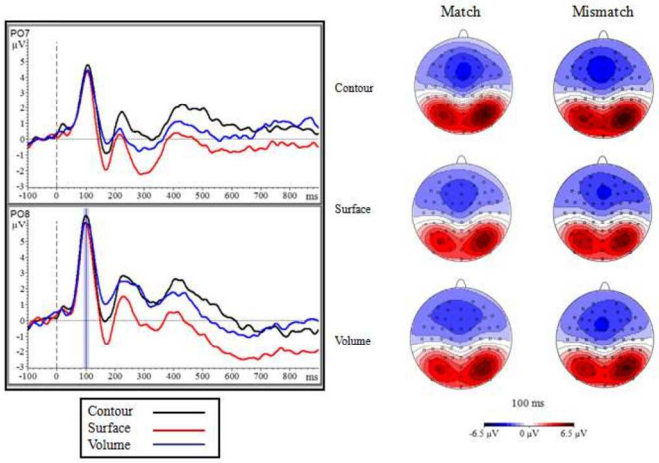

Figure 4

210x297mm (300 x 300 DPI)

FIGURE 5

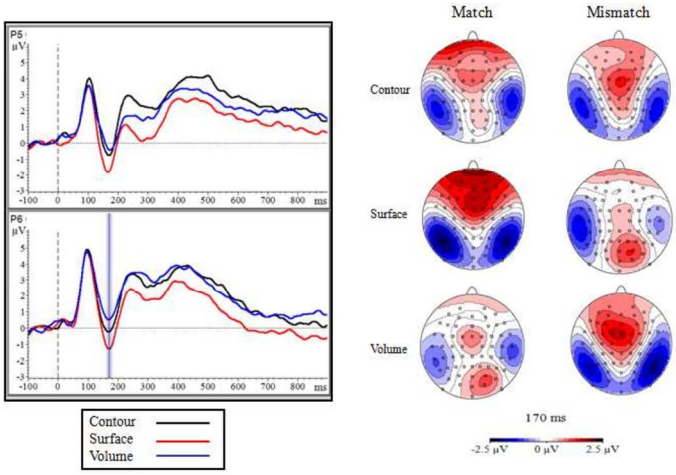

Figure 5

210x297mm (300 x 300 DPI)

FIGURE 6

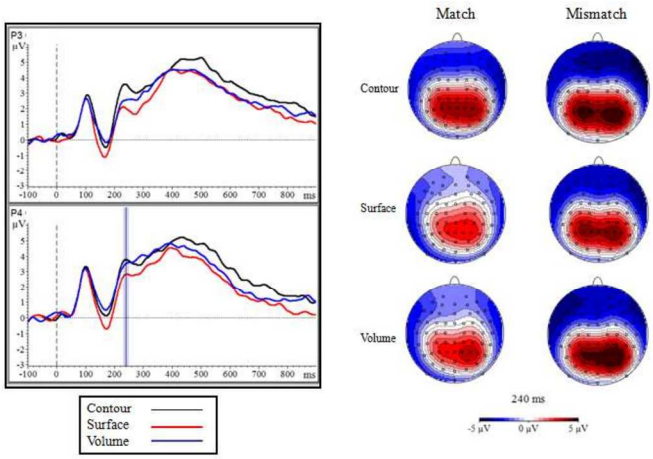

Figure 6

210x297mm (300 x 300 DPI)

FIGURE 7

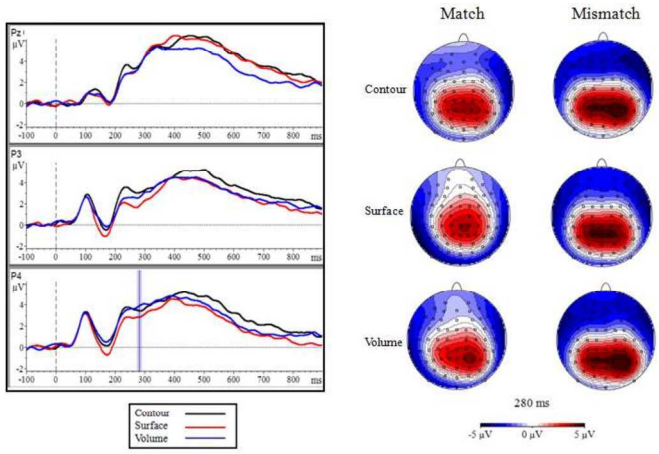

Figure 7

210x297mm (300 x 300 DPI)

FIGURE 8

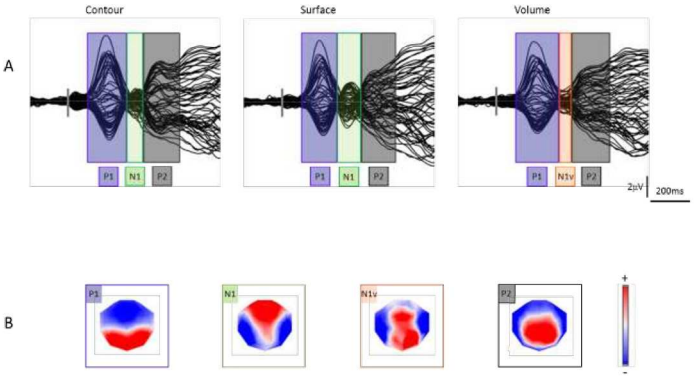

Figure 8

210x297mm (300 x 300 DPI)

FIGURE 9

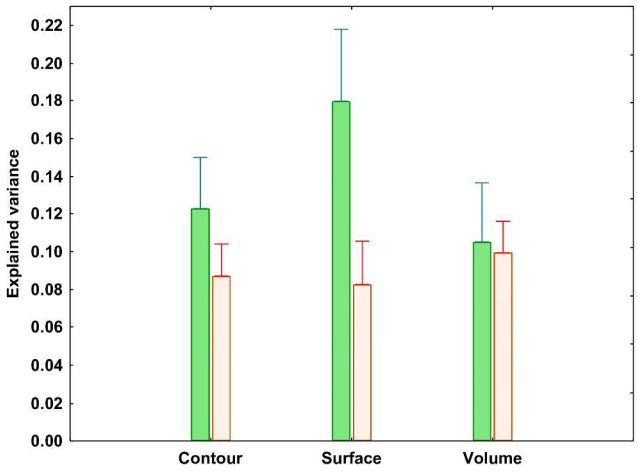

Figure 9

210x297mm (300 x 300 DPI)

FIGURE 10

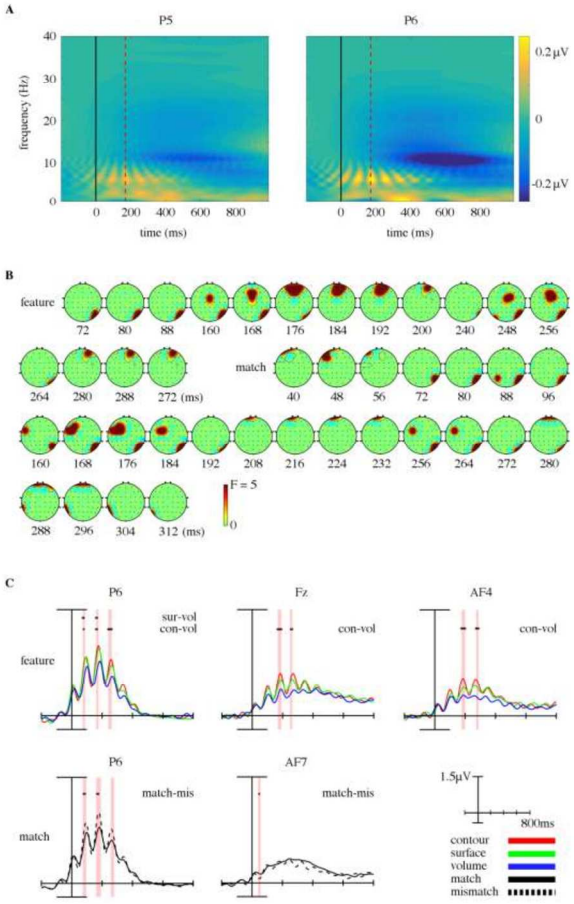

Figure 10

210x297mm (300 x 300 DPI)

FIGURE LEGENDS

Fig 1. The stimulus set used in the current study. Each object (N=12) is shown along with its corresponding matching feature (Contour, Surface, Volume) stimuli.

Fig 2. Illustration of the trial procedure (based on Leek et al., 2005 - Exp 3).

Fig 3. (a) Mean RTs (ms) as a function of feature type (Contour, Surface and Volume) for (correct) match and mismatch trials. Bars show standard error of the mean. **(b)** Difference scores (ms) for Contour (C) versus Surface (S; C-S) and Contour versus Volume (V; C-V) conditions across participants in the match and mismatch trials.

Fig 4. Grand average (match) waveforms (left) and topographies (right) for the **P1** component (70-130ms - highlighted mean peak 100ms) across conditions at electrodes P07 (left hemisphere) and P08 (right hemisphere).

Fig 5. Grand average (match) waveforms (left) and topographies (right) for the **N1** component (140-200ms – highlighted mean peak 170ms) across conditions at electrodes P5 (left hemisphere) and P6 (right hemisphere).

Fig 6 Grand average (match) waveforms (left) and topographies (right) for the **P2** component (220-260ms – highlighted mean peak 240ms) across conditions at electrodes P3 (left hemisphere) and P4 (right hemisphere).

Fig 7. Grand average (match) waveforms (left) and topographies (right) for the **N2** component (260-320ms – highlighted mean peak 280ms) across conditions at electrodes P3 (left hemisphere), Pz (midline) and P4 (right hemisphere).

Fig 8. Results of topographic segmentation of grand average ERPs. A. Grand average ERPs of the matching condition on the 3 conditions are shown for Contour, Surface and Volume, respectively from left to right, with all electrode traces superimposed (inset lower right indicates voltage and time). The vertical grey lines situated on the traces mark the time of stimulus presentation (time 0). Overlaid coloured boxes indicate the time of occurrence of the maps identified in the topographic segmentation. Blue box indicates presence of P1 and black box indicates presence of P2 in the grand averages. The N1 in the volume condition (N1v in brown) differed from the N1 in the other two conditions (N1 in green). B. The map topographies are represented for P1, N1, N1v and P2 (blue, green, brown and black respectively) on a schematised scalp seen from above (forehead on top, left ear on the left). Red regions indicate positive, and blue areas negative regions (see inset on the right).

Fig 9. Amount of variance explained by maps N1 and N1v. The amount of variance (y axis) explained by maps N1 (green) and N1v (brown) during the N1 time period is displayed as a function of experimental condition

Fig 10 Panel A - Event related spectral activity for channel P5 and P6 relative to imperative stimulus onset (time 0; thick black line) for frequency bands from 1 to 40Hz. Spectral activity in each band is extracted using the TSE method (unsmoothed) and normalised to pre-stimulus period. Spikes of activity in the theta band (~6Hz) appear to peak during N1 range (170ms; dashed red line) in both channels, more prominently on the right. Panel B - Topographies from n=100,000 fMax permutation test, for main effects of feature and match on theta (4-7Hz) time courses. Values beneath each topography are latencies, relative to imperative stimulus onset (ms). Topographies show effects of feature on theta power, across right occipitoparietal (OPC: 72-88ms; 160-176ms; 240-264ms), frontal midline (168-192ms; 248-264ms) and right orbitofrontal (OFC: 176-200ms; 272-288ms) sites and effects of match over right OPC site (72-96ms; 160-192ms; 256-280ms), left OFC sites (40-56ms; 208-232; 280-296 ms), and left dorsolateral prefrontal sites (DLPFC: 160-184ms). Panel C - Theta timecourse contrasts. Shaded pink areas display data points where relevant main effect was significant at that channel, while */** display data points where relevant post-hoc tMax contrast was significant. Note that tMax contrasts were only carried out for data points where relevant main effect was significant in the fMax test. Top row shows theta time courses for contour (red), surface (green) and volume (blue) trials, collapsed across match and mismatch, at channels P6 (left), Fz (centre) and AF4 (right). Significantly more right OPC theta power is observed for both surface and contour trials, relative to volume, at a range of data points in the N1 range. Theta power was also significantly higher at frontal sites for contour, relative to volume trials in the N1 range. Bottom row shows theta time courses for match (solid) and mismatch (dashed) trials, collapsed across all feature types, at channels P6 and AF7. Mismatch trials show greater right OPC theta power in the N1 range, while left OFC theta power is significantly higher for match trials in an earlier window (48ms).

Graphical Abstract Text (491 characters with spaces)

This study used event-related potentials to reveal the higher-order structure of three-dimensional object shape representations in human vision. The results showed differential perceptual processing of contour, surface and volumetric shape properties during an N1 component within 140-200ms of stimulus onset. These findings challenge theoretical models that do not attribute functional significance to surface and volumetric part structure during the visual perception of 3D object shape.

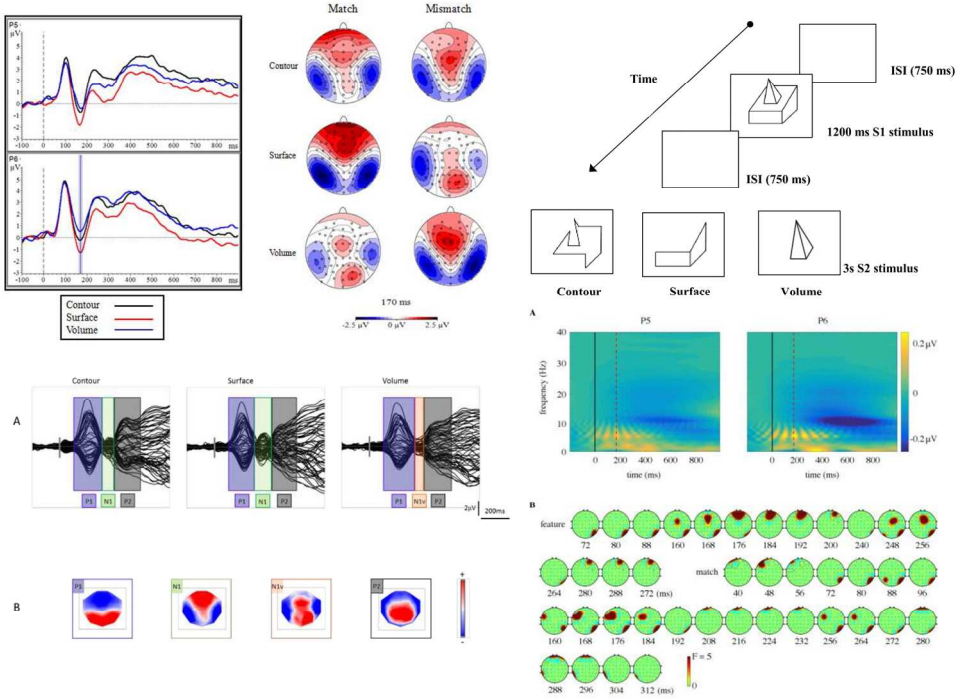
Match
Mismatch
Contour
Surface
Volume
170 ms
-2.5 μV
0 μV
2.5 μV
Contour
Surface
Volume
A
B
Time
ISI (750 ms)
1200 ms S1 stimulus
ISI (750 ms)
3s S2 stimulus
Contour
Surface
Volume
P5
P6
frequency (Hz)
time (ms)
0.2 μV
-0.2 μV
feature
match
272 (ms)
312 (ms)